Title
OPTIMIZATION OF CORROSION RESISTANCE IN METASTABLE AUSTENITIC STEEL.

Author
Padilla, Fred J.

Publication Date
1969-10-01

UCRL-19065

eq 2

OPTIMIZATION OF CORROSION RESISTANCE IN METASTABLE AUSTENITIC STEEL

Fred J. Padilla
(M. S. Thesis)

September 1969

AEC Contract No. W-7405-eng-48

LAWRENCE RADIATION LABORATORY
UNIVERSITY of CALIFORNIA BERKELEY

UCRL-19065

eq 2

DISCLAIMER

TABLE OF CONTENTS

OPTIMIZATION OF CORROSION RESISTANCE IN METASTABLE AUSTENITIC STEEL

Fred J. Padilla

Inorganic Materials Research Division, Lawrence Radiation Laboratory, Department of Materials Science and Engineering, College of Engineering, University of California, Berkeley, California

ABSTRACT

A study has been made leading to the optimization of the mechanical properties and corrosion resistance of metastable austenitic steels. A metastable austenitic steel containing 13% Cr, and 0.25% C was selected as a base composition. Systematic composition changes of the other alloying elements, nickel, molybdenum, and manganese were then carried out.

The effect of these composition changes on the mechanical properties were measured by means of tensile tests. A potentiodynamic polarization technique was used to follow the change in corrosion resistance in a 10% (2.04 Normal) sulfuric acid solution at room temperature.

The steels containing molybdenum exhibited the best combination of mechanical and corrosion-resistant properties. In one of these steels a yield strength of 187 ksi, a tensile strength of 231 ksi, and a 38% elongation were obtained. The corrosion resistance, as determined by the potentiodynamic method, compared favorably with type 304 and type 316 stainless steels. When manganese was substituted for nickel, the mechanical properties were not affected and the corrosion resistance was only slightly decreased.

INTRODUCTION

Experience has shown that in order to achieve high strength, ductility must be sacrificed. In general, a particular steel can be subjected to various heat treatments and deformation processes that will give it either high strength or good ductility, but not both simultaneously.[1] Careful investigation[2] has shown that the brittle behavior of high strength steels is due to a low rate of strain hardening, which causes local plastic instability (necking) and hence, early fracture in a tensile test.

Recent developments[3,4,5,6] have shown that high strength and ductility can be obtained by subjecting metastable austenitic steels to proper combinations of heat treatments and deformation processes (thermomechanical processing). When these materials are strained, they transform from face-centered cubic austenite to body-centered tetragonal martensite. If this transformation begins immediately before necking occurs, a high rate of strain hardening results and the material can continue to deform plastically at high stress levels. Metastable austenitic alloys that exhibit this type of behavior have been called TRIP (Transformation Induced Plasticity) steels.[2]

In order for the material to undergo this austenite-to-martensite transformation, its chemical composition must be properly balanced. The M_s temperature must be below room temperature (or below the test temperature) and the M_d temperature must be above room temperature. (M_d is the temperature below which martensite can be produced by plastic deformation. The M_d temperature is always above the M_s temperature.) The M_s and M_d temperatures are influenced both by chemical composition and thermomechanical processing. It is a generally held concept that after thermomechanical processing the M_s and M_d temperatures increase[3] due at

least in part to some of the carbon being precipitated during processing to form finely dispersed carbides. This decreases the stability of the surrounding austenite. Recently, however, the possibility of the M_s temperature being decreased, while simultaneously the M_d temperature is increased by thermomechanical processing, has been suggested.[7]

A corrosion study on metastable austenitic steels[8] has indicated that these materials undergo an active to passive corrosion behavior similar to stainless steels. A typical TRIP steel, with a nominal composition of 9.0% Cr, 8.0% Ni, 4.0% Mo, 2.0% Mn, 1.0% Si, and 0.25% C, has exhibited a corrosion rate 2 to 3 times greater than an 18% Cr - 8% Ni austenitic stainless steel in 10% sulfuric acid at room temperature. Further investigation indicated that greater corrosion resistance might be possible by increasing the chromium content up to 13%. Other TRIP alloy compositions investigated pointed to a beneficial effect of molybdenum, whereas manganese seemed to be detrimental to corrosion resistance.

The same elements that produce stainless steels, i.e., Cr, Ni, and Mo also influence the stability of the austenite to martensite transformation. By increasing the Cr content to 13%, good corrosion resistance can be anticipated. Commerical stainless steels contain at least 11% Cr.[9] The amount of Ni, Mo, Mn and C must be adjusted to give the desired metastable austenitic structure after thermomechanical processing.

The purpose of this investigation was to determine the influence on the corrosion and mechanical properties of these alloying additions and hence to optimize corrosion resistance with TRIP steel mechanical properties.

II. EXPERIMENTAL PROCEDURE

A. Selection of Alloys

The alloy compositions used in this investigation were selected with the objective of optimizing corrosion resistance with TRIP steel mechanical properties. Previous work[8] enabled the present optimum series to be developed. The chromium content was held constant at 13% (by weight) and the nickel, molybdenum, and manganese contents were systematically varied in order to study their effects on the corrosion and on mechanical properties. The compositions of the series are given in Table I along with the composition of two commerical stainless steels tested, i.e., type 304 and type 316. The M_s temperatures of the alloys, calculated from an empirical equation,[10] are also listed in Table I. The position of the alloys, along with a previously investigated TRIP alloy composition (9% Cr, 8% Ni, 4% Mo, 2% Mn, 1% Si, 0.25% C, Bal. Fe), can be seen in the Modified Schaeffler Diagram[11] of Fig. 1. In this figure the effect of ferrite stabilizers is given by the chromium equivalent and the effect of the austenite stabilizers is given by the nickel equivalent. The calculated M_s temperature, the modified Schaeffler Diagram, and the results of previous work done on metastable austenitic steels[3,12,13,14] were all used as guides in selecting the present alloy compositions.

B. Alloy Processing

Heats of 16-pound ingots were produced by induction melting of high purity elements in a helium atmosphere. (Ingots No. 685-19 and 696-11 were only 8 pound heats.) The ingots were forged at 1100°C into flat bars measuring 3 in. wide by 0.75 in. thick (or 1 in. × 0.625 in. for ingots No. 685-19 and 696-11). The materials were then cross-rolled at 1100°C

to 0.4 in. thick. This was followed by austenitizing the materials at 1200°C for 2-1/2 hours in Sentry-Pac stainless steel bags to prevent decarburization. The material was then quenched in an ice-brine solution. The smaller ingots (No. 658-19 and No. 696-11) were austenitized at 1200°C for 1 hour followed by an ice-brine quench.

The thermomechanical treatment consisted of an 80% reduction in thickness by rolling at 450°C. The material was reheated to 450°C after each pass of 10 to 15 mils. Once a thickness of 0.080 in. was reached, the material was water quenched.

C. Mechanical Testing

Tensile specimens were machined from the 0.080 in. thick as-rolled materials. One inch gage length specimens were used; the specimen dimensions are given in Fig. 2. The tensile tests were carried out at room temperature on an Instron machine using a cross-heat speed of 0.04 in./min.

Rockwell C hardness measurements were made on the tensile specimens before testing, outside of the gage length. Hardness measurements after the tensile test were made within the gage length.

Magnetic measurements were made along the gage length of each specimen before and after the tensile test. A large Crucible hand magnet was used (LRL Stockroom No. 5975-35822).

D. Potentiodynamic Testing

1. Introduction

An electrochemical method of corrosion testing known as the potentiodynamic polarization technique was used in evaluating the corrosion resistance of the alloys. The importance of this method is that it allows a series of alloys, exhibiting passivity, to be systematically tested for

their corrosion properties in a relatively short time (3-4 hours). This method was first proposed by Endeleanu[15] in 1954 and the validity of this technique has since been verified.[8,16-19]

2. The Potentiodynamic Polarization Curve

A typical potentiodynamic anodic polarization curve is shown in Fig. 3. As can be seen, it is a plot of the potential of the metal in an electrolyte (against a standard electrode, such as a calomel electrode) vs. the current density developed by the metal at this potential (with a suitable auxillary electrode, such as platinum). When the potential is slowly, but continuously varied, the resulting plot is called a potentiodynamic curve. When the potential is increased in steps, after being held constant for an arbitrary time, a potentiostatic curve results. Both methods are considered satisfactory,[18] but the speed of the potential sweep does influence the shape of the curve.[20] The curve along the potential axis can be divided into three parts, i.e., (1) active, (2) passive, and (3) transpassive regions.

From this curve it is possible to determine the following:[18,19,21]

(1) The mixed or corrosion potential, E_{corr}: The corrosion potential is the potential of the metal in the environment without any current flowing, i.e., with no dissolution taking place.

(2) The primary passive potential, E_{pp}: Up to the primary passive potential, normal dissolution of the material takes place. As the potential is made more noble, up to the primary passive potential, dissolution of the material increases linearly, a behavior typical of all non-passivating materials. At the primary passive potential the material begins to exhibit a decrease in the dissolution rate (passivation), i.e., the current density decreases. This decrease is thought to be due to the formation of a protective film on the metal surface.

A somewhat effective means of increasing the corrosion resistance of a material is by adding alloying elements which sift the primary passive potential in the active direction.[18] The reason for this is that for chemical passivation to take place, the environment (oxidizing agent) must have a higher (more noble) redox potential than the primary passivation potential of the metal. Hence, the lower (more active) the primary passivation potential of the metal, the greater its corrosion resistance, even in the presence of a weak oxidizing agent, i.e., one that has a low redox potential. In steels, the usual alloying additions of chromium, nickel, and molybdenum generally have only a minor effect on the primary passive potential. Hence, a more important parameter in improving corrosion resistance is the critical current density discussed below.

(3) The critical anodic current density, I_{cr}: The critical anodic current density is the maximum corrosion or dissolution rate of the metal in the environment. It indicates the current that must be achieved in order for the material to passivate. The lower the value of the critical current density, the lower the concentration of oxidizing agents necessary for achieving passivity.[19] Hence, for increased corrosion resistance, alloying additions which lower the critical current density of a material are desirable. This lowering of I_{cr} is generally more effective in increasing passivating tendency than is the altering of the primary passivation potential. The reason for this is that in practical situations, the oxidizing environment (usually containing oxygen) has a redox potential

higher than the primary passivation potential. Therefore, the main barrier to passivation becomes the ability of the environment, by its reduction on the metal, to produce a current density greater than the critical anodic current density.[18,19]

(4) The passive potential region: The passive potential region is indicated by the vertical, low, constant-current-density part of the curve. From a corrosion viewpoint the passive area should be as wide as possible. The material can remain passive under more varied conditions when the primary passive potential (E_{pp}) and the transpassive potential (E_t) are farther apart.

(5) The passive current density, I_p: The passive current density is given by the constant value of the current density in the passive range and indicates the passive corrosion rate. This represents the lowest amount of corrosion taking place. The current density can be related to the corrosion rate by Faraday's Law.[22] Taking into account the percentage of each element in the alloy, an average value of 0.5 mils per year being equivalent to 1μ amp/cm^2 is obtained.[8]

Since the rate of corrosion in the passive state is proportional to the passive current density, increased corrosion resistance can be obtained by lowering the passive current density. Also, the lower the value of I_p, the more stable the passive state becomes.[19] The reason for this is that the lower the passive current density becomes, the less current that must be supplied by the passivating (oxidizing) agent in order to re-

establish a passive film that has been temporarily destroyed.

(6) The transpassive area: In the transpassive area the passive state is destroyed and the current density begins to increase again similar to that in the active region. In some steels a secondary passivity is frequently observed. From a practical standpoint, this secondary passivity is not important due to its small size and instability. Also steels cannot normally reach this high potential except when an external current is supplied. This secondary passivity has been ascribed to the adsorption of oxygen at potentials just before evolution of oxygen in gaseous form occurs.[19]

The above discussion only serves as a guide showing how the anodic polarization curve can be used to systematically follow the effect of composition or other variables on the corrosion properties of an alloy. It is not meant to be a comprehensive explanation of the phenomenon of passivity. Notably missing is the influence of the cathodic reduction curve of the particular alloy in the corrosion system. Detailed discussions have been presented before.[8,15-21]

3. Experimental Technique

Square samples with an approximate surface area of two square centimeters were cut from the 80% deformed materials. Each specimen was mounted in a self-curing resin ("Koldmount") with a No. 21 copper wire soldered onto the back of the specimen. The surface scale was then removed with silicon carbide paper through the 600 grit size, and then the specimen surface was finished by polishing on a 1 micron diamond paste canvas wheel to remove most of the scratches. The specimen was then ultrasonically washed in water and ethyl alcohol, then triply rinsed in ethyl alcohol.

The test solution used was a 10% by weight (2.04 Normal) sulfuric acid solution. It was prepared with distilled water and reagent grade sulfuric acid. The solution was purged with pre-purified (Englehard Deoxo Purifier) hydrogen for 1 hour before placing the specimen in the solution. Hydrogen was passed into the solution continuously throughout the test. The specimen was immersed in the test solution for 15 minutes, prior to the start of the polarization measurement, to establish a steady state corrosion potential. All tests were conducted at a temperature of 22°C ± 1°C.[23]

A polarization cell consisting of three compartments was used as has been described previously.[8] Potentials were measured with reference to a saturated calomel electrode (S.C.E.).

Current signals were fed through a logarithmic converter with a resistance selector switch attached. This enabled uninterrupted recording of polarization currents from 0.5 to 10^6 μ amps. A low-pass filter was employed which reduced extraneous electrical noise in the electrochemical circuit and provided smooth experimental curves.[24] Current values along with the corresponding potential values were then fed into a X-Y recorder.

Polarization measurements were begun at the corrosion potential,[20] and potentials were scanned automatically with the aid of a geared motor[8] at the rate of 1.3 volts per hour.

The equipment used was as follows:

Potentiostat: Magna-Anotrol Model 4700M

Logarithmic Converter: Moseley Model 7561-A

X-Y Recorder: Moseley Model 2D-2

Resistance Selector Switch: Based on the log converter input

voltage requirements of 0.00316 to 3.16 volts, the recordable current ranges for the specified precision resistors (±1%) used were as follows:

2 ohm	10^3 - 10^6 μ amps
200 ohm	10 - 10^4 μ amps
20,000 ohm	0.2 - 10^2 μ amps

The resistance selector switch was activated by microswitches attached to the recorder chassis at selected positions along the X-axis.

Low-Pass RC Filter: A 100μ f capacitor in parallel with a 25K potentiometer, adjusted to 10K, gave a suitable time constant of 1 second.

III. EXPERIMENTAL RESULTS AND DISCUSSION

A. Mechanical Tests

The only variable in all of these alloys was chemical composition. All other processing and testing factors were held constant, i.e., austenitizing temperature (1100°C), deformation temperature (450°C), amount of deformation (80%), and testing temperature (22°C). The mechanical properties of the alloys indicate that the resulting structures ranged from metastable to completely stable austenite. A summary of these properties is given in Table II along with values from the literature for type 304 and type 316 stainless steel. Alloys A, E, F, G and H were sufficiently metastable to undergo the TRIP phenomenon, and excellent strength-ductility values were obtained. The austenite in alloys D and I was metastable and underwent the austenite to martensite transformation, but at an insufficient rate to show appreciable strain-hardening (TS/YS ratios of 1.05 and 1.01 respectively).

Alloys A, D, F, G and H were assumed to be completely austenitic before testing as indicated by their non-magnetic behavior. The remaining alloys were slightly magnetic before testing, indicating a small amount of martensite was present.[25] The calculated M_s temperature for these alloys (B, C, E, and I) were all above 80°C, indicating that some martensite may have been formed by quenching after austenitizing.

All of the alloys which underwent the austenite to martensite transformation exhibited a sharp yield point and Luders' strain. After the Luders' strain, the slope of the stress-strain curve increased and a number of serrations appeared. These serrations have been attributed to the formation of martensite in local necked regions of the specimen. Due

to the higher strain in these regions, martensite forms and strengthens this region against further necking. Martensite is a more effective barrier to dislocation motion, hence deformation then proceeds in other areas of the specimen.[4] These serrations may also be due to the Portevin-LeChatelier effect as has been suggested by other investigations of metastable austenitic[26] and ausformed steels.[27] The Portevin-LeChatelier effect probably plays only a minor role in the materials examined here due to the low diffusion rate of the solute elements at room temperature.[28]

The difference between alloys A and B was that alloy B contained 2.7% more Ni. Alloy B had a higher yield point, probably because of a combination of solution hardening and the fact that a small amount of martensite was initially present in alloy B. This martensite may have been produced either by the quenching after austenitizing or during deformation of the austenite at 450°C. Since the material behaved in a somewhat ductile manner, showing cup-cone fracture and 8% elongation, its non-TRIP behavior was probably due to the stability of the austenite against transformation by straining, and not to the initial martensite present. The influence of composition alone on the stability of the austenite in alloy B is indicated by its higher position in the Modified Schaeffler Diagram Fig. 1.

Comparing alloys B, C, D, F, and G it is seen that as Mo is added and Ni decreased, a more unstable austenite is produced. This leads to excellent strength-ductility values as a result of the strengthening action of the austenite-to-martensite transformation. The increase in yield strength of alloys B, C, and D may be due to a combination of solution-hardening by the Mo, and hardening by precipitates of molybdenum carbides. At a Mo/Ni ratio of 3/8 (alloy F) the yield strength drops, and at a ratio of 4/7 (alloy G) the yield strength slightly decreases again.

This indicates that the beneficial efforts of solution and precipitation hardening may have been reached.

Comparing alloys F and H it is seen that Mn can be directly substituted for Ni. The two alloys have approximately the same mechanical properties.

No definite relationship could be established between the position of the alloy in the Modified Schaeffler Diagram, its calculated M_s temperature, and its mechanical properties. In general, though, it was observed that if the position of the alloy was too far above the austenite-martensite boundary in the Modified Schaeffler Diagram the TRIP phenomenon did not occur . As mentioned before the Modified Shaeffler Diagram and the calculated M_s temperature are used only as guides in selecting compositions that may undergo the transformation from austenite to martensite after yielding of the material takes place. These two guides do not take into consideration the effect that the thermomechanical processing has on M_s and M_d, and hence on the resulting mechanical properties.

B. Potentiodynamic Studies

The complete polarization curves obtained for the alloys studied are given in Figs. 4 to 14. All potentials are reported as volts vs. a saturated calomel electrode (S.C.E.). If the potentials vs. the normal hydrogen electrode are desired, 0.245 must be added to the S.C.E. values. The effects of Ni, Mo, and Mn on the electrochemical parameters are summarized in Table III. For comparison, the electrochemical values obtained for type 304 (1/16 inch thick) and type 316 (1/8 inch thick) stainless steel sheet are also listed in Table III. The polarization curves obtained for type 304 (Fig. 13) and type 316 (Fig. 14) stainless steels compared favorably with previously published results.[21,23,24] This indicates that the

procedures used in this report are consistent with those used by other investigators. The electrochemical parameters listed in Table III are the primary passive potential, E_{pp}, the critical anodic current density, I_{cr}, and the passive corrosion current density, I_p. The effect of the alloying elements was most pronounced in the active region, where significant changes were observed in the critical current density, I_{cr}, and the corresponding potential, E_{pp}. Current density in the passive state, I_p, was approximately the same for all the experimental materials. It ranged from a minimum of 7 $\mu a/cm^2$ (Alloy F) to a maximum of 13 $\mu a/cm^2$ (Alloy E). The critical current density, I_{cr}, on the other hand, ranged from a low value of 12 $\mu a/cm^2$ (Alloy G) to a high value of 960 $\mu a/cm^2$ (Alloy A). The mixed or natural corrosion potential, E_{corr}, of the alloys is indicated on the polarization curves. The passive potential region for all alloys ranged from approximately +0.1 V. to +0.95 V. The passive potential region was slightly larger for the alloys containing greater amounts of Mo.

1. The Effect of Nickel

The influence of Ni is seen by comparing alloys A and B (Fig. 4 and 5). The extra 2.7% Ni in alloy B decreased I_{cr} from 960 $\mu a/cm^2$ to 720 $\mu a/cm^2$ and I_p from 11 $\mu a/cm^2$ to 9.5 $\mu a/cm^2$. As expected E_{corr} and E_{pp} became slightly more positive.[29] It was previously mentioned that alloy B was slightly magnetic, which would indicate that a small amount of martensite might be present. This did not seem to appreciably affect the shape of the polarization curve in the passive range. The effect of Ni on the mechanical properties, however, was significant as discussed previously. Photomicrographs taken of each alloy after the curve was obtained are shown in Fig. 15 and 16 for alloys A and B respectively. A greater amount of intergranular corrosion can be seen for alloy A. This does not necessarily

imply that alloy A is more susceptible to intergranular corrosion, since the usefulness of the potentiostatic method for investigation of intergranular corrosion has not yet been established.[30-32]

2. The Effect of Molybdenum and Nickel

The influence of the Mo/Ni ratio can be seen by comparing alloys B, C, D, F, and G. The Mo content was increased by 1% steps as the Ni was decreased by the same amount for this series. The nominal Mo/Ni ratios for the above alloys are as follows:

	Nominal Composition Weight Per Cent			E_{pp}	I_{cr}	I_p
Alloy	Cr	C	Mo/Ni	V vs S.C.E.	$\mu amp/cm^2$	
B	13.0	0.26	0/11	-0.32	720	9.5
C	13.0	0.26	1/10	-0.31	98	11
D	12.6	0.25	2/9	-0.27	35	12
F	12.3	0.24	3/8	-0.24	17	7
G	12.9	0.25	4/7	-0.25	12	9.5

As can be seen, there is a tendency toward more positive primary passive potentials, E_{pp} as the Mo is increased and Ni decreased. The outstanding effect that Mo has is in decreasing the critical anodic current density, I_{cr}. This observation is in agreement with other investigations.[18,19,21] Comparing alloys B and C, it is seen that a very large decrease in I_{cr} is obtained by the simultaneous decrease of Ni by 1% and increase of Mo by 1%. I_{cr} is decreased by at least half of the previous value in going from a Mo/Ni ratio of 1/10 to 2/9 and from 2/9 to 3/8. When this ratio is changed from 3/8 to 4/7, I_{cr} only decreases by one-third. This seems to indicate that a leveling effect is beginning to take place. The ex-

tent of the passive range also seems to have been maximized at a Mo/Ni ratio of 4/7 as can be seen from an examination of the polarization curves.

Molybdenum has been used to decrease the susceptibility of 18% Cr - 8% Ni (type 304) stainless steel to pitting. The reason for its success is "apparently due to a more protective or more stable passive surface."[33] This apparent increase in the stability of the passive film (lower I_{cr}) has been found to be true in the 13% Cr steels investigated. This would indicate that alloys F or G, which have the lowest I_{cr}, may have a high resistance to pitting.

The passive current density, I_p, of alloys C(1/10) and D(2/9) increased slightly over that of alloy B (0/11). Alloy F with a Mo/Ni ratio of 3/8 showed a decrease of I_p to a value of 7 $\mu a/cm^2$. This was the lowest passive current density obtained for all the alloys tested. This corresponds to a corrosion rate of approximately 3.5 mils per year in the passive range. Examination of the table given above shows that with an increase of the Mo/Ni ratio to 4/7 (Alloy G), an increase in I_p to the value of alloy B (0/11) takes place. This seems to indicate that the beneficial effect of Mo/Ni is best at a ratio of 3/8 (Alloy F).

Photomicrographs of these alloys are shown in Figs. 16 through 20. These were taken immediately after each polarization curve was obtained. The distorted austenitic structure caused by the thermomechanical processing is clearly visible (relief markings) as well as the chromium and molybdenum carbides. Figures 14 (Alloy B) and 18 (Alloy G) show the greatest corrosion on grain boundaries and have a similar appearance. This may be an indication, as was mentioned previously in discussing the effect of Mo/Ni ratio on I_{cr} and I_p, that the beneficial effect of Mo may have been reached at a Mo/Ni ratio of 3/8 (Alloy F). Any further increase in the Mo content may not be able to compensate for the loss in Ni.

3. The Effect of Molybdenum

The influence of Mo on alloys with a fixed Ni content of 8% can be seen by comparing alloys A, E, and F. The values obtained for the primary passivation potential, E_{pp}, critical current density, I_{cr}, and the passive current density I_p are given below, as well as in Table III.

	Composition, wt.%				E_{pp}	I_{cr}	I_p
Alloy	Cr	Ni	C	Mo	V vs S.C.E.	$\mu amps/cm^2$	
A	12.9	7.8	0.26	-	-0.34	960	11
E	13.4	7.6	0.21	1.0	-0.32	76	13
F	12.3	7.8	0.24	3.0	-0.24	17	7

As can be seen in the table above a 1% addition of Mo resulted in a very large decrease in I_{cr}. The addition of Mo to 3% caused a further reduction of I_{cr} to a value of 17 $\mu a/cm^2$. The value of I_p actually increased slightly with the addition of 1% Mo, but decreased to the lowest value of all alloys tested when the Mo was increased to 3%. By examining the polarization curves (Figs. 4,8,9) for these three alloys one can see the increase in the stable passive potential range for alloy F over alloys A and E.

Alloy F compares very favorably with both types of stainless steels tested. This can be seen in the table below (or in Table III).

Alloy	Composition, wt.% Cr	Ni	Mo	Mn	C	Fe	E_{pp} V vs S.C.E.	I_{cr} μamp/cm²	I_p
F	12.3	7.8	3.0	-	0.24	Bal.	-0.24	17	7
304	20.0	9.1	-	1.8	0.08	Bal.[a]	-0.22	84	4
316	18.0	13.5	3.0	1.0	0.04	Bal.[a]	-0.18	16	4

[a] This alloy also contains a maximum of 1.00% silicon, 0.045% phosphorus and 0.030% sulfur.

The value of I_{cr} was much lower for Alloy F than for type 304 stainless steel. This indicates that a much lower current (or lower concentration of oxidizing agent) is required in order to achieve passivity with Alloy F or type 316 stainless steel. Once passivity is achieved, type 304, and type 316 stainless steels will corrode at a slightly lower rate than Alloy F. The lower value of I_p for the stainless steels as compared to Alloy F is due to their higher chromium content.

All of the alloys tested, including type 304 and type 316 stainless steels indicate that their passive corrosion rate is well under 20 mpy. According to the report "Corrosion Data Survey,"[36] this is the maximum corrosion rate which would enable a material to be used in a process with only minor maintenance.

Actual long term corrosion studies in the same reference[36] show that an 18% Cr-8% Ni stainless steel corrodes at a rate of 50 miles per year, whereas type 316 stainless steel corrodes at a rate less than 20 mils per year. This is in an air-free, 10% sulfuric acid solution at room temperature. Since the polarization curve for alloy F is very similar to the curve for type 316, it can be expected that alloy F might behave in a similar manner as type 316 stainless steel.

4. The Effect of Manganese

The influence of Mn can be seen by comparing alloys H, I and F listed below or in Table III.

Alloy	Composition, wt.% Cr	Ni	Mo	Mn	C	E_{pp} V vs S.C.E.	I_{cr} μamps/cm^2	I_p
H	13.0	5.9	3.0	2.0	0.25	-0.28	30	9.5
I	12.8	5.8	3.0	4.0	0.185	-0.38	38	8.5
F	12.3	7.8	3.0	-	0.24	-0.24	17	7

Alloys H and I were identical in composition except for the Mn. The major effect of Mn was in increasing the critical current density, I_{cr} and hence decreasing the stability and ease of achieving passivity. Comparison of alloy H with F, which has the same Nickel Equivalent, i.e., austenite forming elements (Ni, Mn, C) and the same mechanical properties, shows that I_{cr} is approximately doubled by the addition of 2% Mn. Addition of Mn up to 4.0% (Alloy I) caused a further increase in I_{cr}, but due to the lower carbon content of this alloy, the increase is not very large. The passive current density, I_p, also increased slightly over those alloys without Mn. The potential range of the passive region was not greatly affected by the Mn additions.

Comparing alloy H(2% Mn) with type 304 stainless steel (Table III) shows that, even with the manganese addition, the critical current density, I_{cr} of alloy H remained twice as low as for type 304 stainless steel.

The corrosion parameters with Mn additions for a high purity austenitic steel (14 Cr - 14 Ni - Bal. Fe) have recently been investigated.[35] A much greater increase in I_{cr} and I_p was noted that with the steels investigated in this report. The probable reason for the greater

increase in the corrosion parameters of the high purity austenitic steel was due to the lack of molybdenum in this steel.

IV. SUMMARY AND CONCLUSIONS

The effects of composition on the mechanical and corrosion properties of a new series of metastable austenitic steels have been determined. A summary of these properties can be found in Table IV. The base composition for this series was 13% Cr and 0.25%C with the balance being iron.

The conclusions arrived at are as follows:

1. The increase of chromium to 13% provided the basis for metastable austenitic steels with greatly improved corrosion resistance and similar mechanical properties compared to the 9% chromium TRIP steels.

2. The tensile properties were dependent on the effect that the composition had on stabilizing the austenite. If the austenite was too stable, the transformation from austenite to martensite during straining did not occur. The alloys with compositions close to the austenite martensite boundary in the Modified Schaeffler Diagram (Fig. 1) underwent the TRIP phenomenon.

3. Increasing molybdenum in a steel of fixed nickel content (Alloys A, E, and F) resulted in outstanding improvement in corrosion properties, i.e., ease of achieving passivity and low passive corrosion rate.

4. Nickel also improved the corrosion resistance of these steels but not to the extent shown by molybdenum (Alloys A and B).

5. Molybdenum combined with nickel exerts a powerful influence on the mechanical and the corrosion properties of metastable austenitic steels. A Mo/Ni ratio of 3/8 (Alloy F) or 4/7 (Alloy G) yielded the best corrosion resistance.

6. Manganese was seen to slightly increase the critical current density and the passive current density. Nevertheless, the alloy with 2%

Mn substituted for an equivalent amount of Ni (Alloy H), achieved passivity with greater ease (lower critical current density) than type 304 stainless steel. This was undoubtedly due to the presence of molybdenum in Alloy H. Also chromium had an overriding effect, since the 13% chromium steel with 2% manganese exhibited a passive corrosion rate twice as low as a 9% chromium steel with 2% manganese previously investigated.

7. The optimum combination of mechanical and corrosion properties are given by a Mo/Ni ratio of 3/8 (Alloy F) or 4/7 (Alloy G). Alloy F in particular exhibits corrosion properties comparable to type 304 and type 316 stainless steels. The 13% chromium TRIP steels have passive corrosion rates two to five times better than the 9% chromium TRIP steels previously investigated.

8. The use of a log converter, resistance selector switch, and a low pass filter in the experimental apparatus greatly improved the recording and interpretation of the potentiodynamic polarization curves. Confidence in the validity of using this equipment was established by obtaining polarization curves similar to those obtained by other investigations for type 304 and type 316 stainless steels.

V. RECOMMENDATIONS FOR FUTURE WORK

In order to investigate fully the properties and potential usefulness of the materials examined more work needs to be carried out.

1. The mechanical properties should be studied at different temperatures. This will give more information as to the effect of the composition and thermomechanical processing on the M_s and M_d temperatures.

2. Other mechanical tests, such as fracture and impact toughness, and fatigue should be initiated. Preliminary results on alloy D under plane stress conditions at room temperature, indicate that a fracture toughness value of over 170 ksi - $in^{1/2}$ can be expected.

3. The materials should be potentiodynamically tested to check the influence of temperature. Likewise, resistance to pitting in various media containing chlorides can be tested.

4. Potentiodynamic curves should be run after the material has been partially and completely transformed to martensite under strain to check the effects on corrosion resistance. This will also be useful for selective potentiostatic etching of austenite or martensite since each phase has its own characterisitic polarization curve.

5. Standard corrosion and stress-corrosion tests, both short term and long term, in various media should be started.

6. Standardization of the potentiodynamic technique following the recommendations of the ASTM G-1/XI. Interlaboratory Testing Program (June 29, 1967, prepared by Task Group 2, to be published) would be advisable.

7. In order to obtain a more basic understanding of the influence of molybdenum in the passive film formation, work might be initiated

utilizing the microprobe, scanning and electron microscopes, and an ellipsometric technique.[37]

ACKNOWLEDGEMENTS

The author would like to express his grateful appreciation to Professors E. R. Parker, S. F. Ravitz, and V. F. Zackay for their encouragement and guidance throughout the course of this investigation. Thanks are also due to Mr. W. W. Gerberich and Dr. R. Muller for their helpful discussions and advice.

I would like to express my thanks to the many staff members of the Inorganic Materials Laboratory, without whom this work could never have been completed.

This work was performed under the auspices of the United States Atomic Energy Commission through the Inorganic Materials Research Division of the Lawrence Radiation Laboratory, Berkely, California.

REFERENCES

1. Zackay, V. F., and Parker, E. R., High Strength Materials, p. 130, Zackay, V. F., Ed., (John Wiley and Sons, New York, 1965).

2. Parker, E. R. and Zackay, V. F., High Strength Steels - Present Status and Future Prospects, UCRL-18699, Jan. 1969.

3. Zackay, V. F., Parker, E. R., Fahr, D., and Busch, R., The Enhancement of Ductility in High Strength Steels, ASM Trans. 60, 252 (1967).

4. Bressanelli, J. P. and Moskowitz, A., Effects of Strain Rate, Temperature and Composition on Tensile Properties of Metastable Austenitic Stainless Steels, ASM Trans. Quart. 59, 223 (1966).

5. Banerjee, B. R., Capenos, J. M., and Hauser, J. J., Fracture Mechanics of Extra-Work-Hardened Type 301 Stainless, in Application of Fracture Toughness Parameters to Structural Metals, Greenberg, Ed., (Gordon and Breach Co., 1966).

6. Kula, E. B., Strengthening of Steel by Thermomechanical Treatments, in Strengthening Mechanisms, Proceedings of the 12th Sagamore Army Materials Research Conference, Syracuse University Press (1966).

7. Zackay, V. F., Some Anticipated Developments in Physical Metallurgical Research, UCRL-18676, p. 16, Jan. 1969.

8. Challande, J. F., Corrosion Resistance of Metastable Austenitic Steels, M.S. Thesis, University of California, Berkeley, Sept. 1968.

9. Fontana, M. G., and Greene, N. D., Corrosion Engineering, p. 163 (McGraw-Hill Book Co., New York, 1967).

10. Proposal: Study of Diffusion, Precipitation, and Strengthening in Alloys Utilizing the Portenin-LeChatelier Effect, Publication No. P-24083(U), Philco Research Laboratories (1964).

11. Rollason, E. C., Fundamental Aspects of Molybdenum on Transformation of Steel, (Climax Molybdenum Company of Europe, Ltd., London, England, 1962).

12. Fahr, D., Strengthening Mechanisms of Ultra-High-Strength Austenitic Steel, M.S. Thesis, University of California, Berkeley, June 1966.

13. Dunning, J. S., The Microstructure and Properties of Metastable Austenitic High Strength Steels, M.S. Thesis, University of California, Berkeley, December 1966.

14. Chanani, G. R., The Strength and Ductility of Metastable Austenitic Steels as a Function of Composition and Test Temperatures, M.S. Thesis, University of California, Berkeley, September 1967.

15. Endeleanu, C., Method for the Study of Corrosion Phenomena, Nature, 173, 739 (1954).

16. Endeleanu, C., A Potentiostat Technique for Studying the Acid Resistance of Alloy Steels, J. Iron and Steel Inst., 188, 122 (1958).

17. Greene, N. D., The Classical Potentiostat: Its Application to the Study of Passivity, Corrosion, 15, 369t (1959).

18. Greene, N. D., Predicting Behavior of Corrosion Resistant Alloys by Potentiostatic Polarization Methods, Corrosion, 18, 136t (1962).

19. Prazak, M., Evaluation of Corrosion-Resistant Steels Using Potentiostatic Polarization Curves, Corrosion, 19, 75t (1963).

20. Greene, N. D. and Lenard, R. B., Comparison of Potentiostatic Anodic Polarization Methods, Electrochimica Acta, 9, 45 (1964).

21. Fontana, M. G., and Greene, N. D., Corrosion Engineering, 319-324, 335-338, (McGraw-Hill Book Co., Inc., New York, N. Y., 1967).

22. Potter, E. C., Electrochemistry - Principles and Applications, 7-9, (Cleaver-Hume Press Ltd., London, 1956).

23. Greene, N. D., Experimental Electrode Kinetics,(Rensselaer Polytechnic Institute, Troy, N. Y., 1965).

24. France, Jr., W. D., and Lietz, R. W., Improved Data Recording for Automatic Potentiodynamic Polarization Measurements, 24, 298 (1968).

25. Miramon, B., Quantitative Investigation of Strain Induced Strengthening in Steel, M.S. Thesis, University of California, Berkeley, September, 1967.

26. Gerberich, W. W., Martin, C. F., and Zackay, V. F., Serrated Stress-Strain Curves of Metastable Austenite in Alloy Steels, ASM. Trans. 58, 85 (1965).

27. Thomas, G., Schmatz, P., and Gerberich, W., Structure and Strength of Some Ausformed Steels, p. 251, in High Strength Materials, ed., Zackay, V. F., (John Wiley and Sons, New York, N. Y., 1965).

28. Adsit, N. R. and Lautenschlager, E. P., Strain Aging in the Blue Brittleness Region, ASM Trans. 56, 197 (1963).

29. Meyers, J. R., et al., Anodic Polarization Behavior of Nickel-Chromium Alloys in Sulfuric Acid Solutions, Corrosion, 21, 277 (1965).

30. France, Jr., W. D., and Greene, N. D., Interpretation of Passive Current Maxima During Polarization of Stainless Steels, Corrosion, 24, 403 (1968).

31. France, Jr., W. D. and Greene, N. D., Predicting the Intergranular Corrosion of Austenitic Stainless Steels, Corrosion Science, 8, 9 (1968).

32. Streicher, M. A., The Time-Factor in Potentiostatic Studies of Intergranular Corrosion of Austenitic Stainless Steel, Corrosion Science, 9, 53 (1968).

33. Fontana, M. G., and Greene, N. D., Corrosion Engineering, p. 57, (McGraw-Hill Book Company, New York, N. Y., 1967).

34. Littlewood, R., The Effect of Variations in Technique on Polarization Curves Obtained with a Potentiostat, Corrosion Science, 3, 99 (1963).

35. Wilde, B. E. and Armigo, J. R., Influence of Silicon and Manganese on Corrosion Behavior of Austenitic Stainless Steels, Corrosion, 24, 393 (1968).

36. Nelson, G. A., Corrosion Data, Survey, pp. 6 and S-9, (Shell Development Company, Emeryville, California, 1960).

37. Kruger, J., Use of Ellipsometry in the Study of Corrosion, Corrosion, 22, 88 (1966).

Table I. Chemical composition of alloys in weight percent

Ingot No.	Alloy	Cr	Ni	Mo	Mn	C	Fe	Calculated M_s (C°)
685-19	A	12.9	7.8	-	-	0.26	Bal.	128
6811-3	B	13.0	10.5	-	-	0.26	Bal.	80
6811-4	C	13.0	10.0	1.0	-	0.26	Bal.	89
6811-6	D	12.6	8.8	2.0	-	0.25	Bal.	74
696-11	E	13.4	7.6	1.0	-	0.236	Bal.	116
6811-7	F	12.3	7.8	3.0	-	0.24	Bal.	72
6811-8	G	12.9	6.9	4.0	-	0.25	Bal.	55
6811-9	H	13.0	5.9	3.0	2.0	0.25	Bal.	19
6811-10	I	12.8	5.8	3.0	4.0	0.185	Bal.	-29
	304	18.7	9.1	-	1.8	0.08	Bal.[a]	
	316	18.0	13.5	3.0	1.0	0.04	Bal.[a]	

[a] This alloy also contains a maximum of 1.00% silicon, 0.045% phosphorus and 0.030% sulfur.

Table II. Mechanical properties

Alloy	Yield strength ksi	Tensile strength ksi	T.S./Y.S.	% Elong. 1 inch	% Red. in area	R_c Hardness Before Test[a]	R_c Hardness After Test[b]	Magnetic Characteristic[b] Before Test	Magnetic Characteristic[b] After Test
A	164	253	1.54	28	32	48	55	Non-Mag.	Mag.
B	187	187	1.0	8	51	41	41	Sl-Mag.	Mag.[c]
C	194	194	1.0	11	51	42	42	Sl-Mag.	Mag.[c]
D	200	209	1.05	46	44	45	55	Non-Mag.	Mag.
E	190	264	1.39	27	35	48	56	Sl-Mag.	Mag.
F	187	231	1.24	38	38	45	57	Non-Mag.	Mag.
G	185	249	1.35	34	42	49	58	Non-Mag.	Mag.
H	185	231	1.25	40	33	44	57	Non-Mag.	Mag.
I	186	188	1.01	46	42	44	52	Sl-Mag.	Mag.
304[d]	35[e]	85	2.42	55[f]	65	80	-	Non-Mag.	-
316[d]	35[e]	85	2.42	55[f]	70	80	-	Non-Mag.	-

[a] Outside gage length of specimen.

[b] Within gage length of specimen.

[c] Magnetic around necked area only.

[d] Values of mechanical properties taken from Metals Handbook, Vol. 1, 8th edition, 1961.

[e] 0.2% offset yield strength value.

[f] 2 inch gage length.

Table III. Effect of Ni, Mo, Mn, on anodic polarization behavior

Ingot No.	Alloy	Cr	Ni	Mo	Mn	C	Fe	E_{pp}[a] V vs S.C.E.	I_{cr}[b] $\mu a/cm^2$	I_p[c] * $\mu a/cm^2$
			weight percent							
685-19	A	12.9	7.8	-	-	0.26	Bal.	-0.34	960	11
6811-3	B	13.0	10.5	-	-	0.26	Bal.	-0.32	720	9.5
6811-4	C	13.0	10.0	1.0	-	0.26	Bal.	-0.31	98	11
6811-6	D	12.6	8.8	2.0	-	0.25	Bal.	-0.27	35	12
696-11	E	13.4	7.6	1.0	-	0.236	Bal.	-0.32	76	13
6811-7	F	12.3	7.8	3.0	-	0.24	Bal.	-0.24	17	7
6811-8	G	12.9	6.9	4.0	-	0.25	Bal.	-0.25	12	9.5
6811-9	H	13.0	5.9	3.0	2.0	0.25	Bal.	-0.28	30	8.5
6811-10	I	12.8	5.8	3.0	4.0	0.185	Bal.	-0.38	38	9.5
	304	18.7	9.1	-	1.8	0.08	Bal.[d]	-0.22	84	4
	316	18.0	13.5	3.0	1.0	0.04	Bal.[d]	-0.18	16	4

[a] E_{pp} = Primary passive potential.

[b] I_{cr} = Critical anodic current density.

[c] I_p = Passive corrosion current density.

[d] This alloy also contains a maximum of 1.00% silicon, 0.045% phosphorus and 0.030% sulfur.

* 1 $\mu a/cm^2 \simeq$ 0.5 mils per year.

Table IV. Summary of anodic polarization results and mechanical properties[a]

Ingot No.	Alloy	Cr	Ni	Mo	Mn	C	Fe	E_{pp}[b] V vs S.C.E.	I_{cr}[c] $\mu a/cm^2$	I_p[d] * $\mu a/cm^2$	Yield[e] strength ksi	Tensile strength ksi	% Elong.[f] 1 in.
				weight percent									
685-19	A	12.9	7.8	-	-	0.26	Bal.	-0.34	960	11	164	253	28
6811-3	B	13.0	10.5	-	-	0.26	Bal.	-0.32	720	9.5	187	187	8
6811-4	C	13.0	10.0	1.0	-	0.26	Bal.	-0.31	98	11	194	194	11
6811-6	D	12.6	8.8	2.0	-	0.25	Bal.	-0.27	35	12	200	209	46
696-11	E	13.4	7.6	1.0	-	0.236	Bal.	-0.32	76	13	190	264	27
6811-7	F	12.3	7.8	3.0	-	0.24	Bal.	-0.24	17	7	187	231	38
6811-8	G	12.9	6.9	4.0	-	0.25	Bal.	-0.25	12	9.5	185	249	34
6811-9	H	13.0	5.9	3.0	2.0	0.25	Bal.	-0.28	30	8.5	185	231	40
6811-10	I	12.8	5.8	3.0	4.0	0.185	Bal.	-0.38	38	9.5	186	188	46
	304	18.7	9.1	-	1.8	0.08	Bal.[g]	-0.22	84	4	35	85	55
	316	18.0	13.5	3.0	1.0	0.04	Bal.[g]	-0.18	16	4	35	85	55

[a] Mechanical properties for type 304 and type 316 taken from the Metals Handbook, 1961.

[b] E_{pp} = Primary passive potential.

[c] I_{cr} = Critical anodic current density.

[d] I_p = Passive corrosion current density

[e] 0.2% offset yield strength for type 304 and type 316 stainless steels.

[f] 2 inch gage length for type 304 and type 316 stainless steels.

[g] This alloy also contains a maximum of 1.00% silicon, 0.045% phosphorous and 0.030% sulfur.

* 1 $\mu amp/cm^2 \approx 0.5$ mils per year.

FIGURE CAPTIONS

Fig. 1 Modified Schaeffler Diagram. The positions of the alloys tested are indicated. A typical 9% Cr TRIP steel is indicated by a bullet (•).

Fig. 2 Tensile specimen used in the determination of mechanical properties.

Fig. 3 Schematic anodic polarization curve of an active-passive metal.

Fig. 4 Experimentally obtained anodic polarization curve for Alloy A (685-19). The break marks in the curve indicate where the resistance selector switch was automatically activated in order to continue recording the increasing or decreasing current.

Fig. 5 Experimentally obtained anodic polarization curve for Alloy B, (6811-3). The break marks in the curve indicate where the resistance selector switch was automatically activated in order to continue recording the increasing or decreasing current.

Fig. 6 Experimentally obtained anodic polarization curve for Alloy C (6811-4). The break marks in the curve indicate where the resistance selector switch was automatically activated in order to continue recording the increasing or decreasing current.

Fig. 7 Experimentally obtained anodic polarization curve for Alloy D (6811-6).

Fig. 8 Experimentally obtained anodic polarization curve for Alloy E (696-11). The break marks in the curve indicate where the resistance selector switch was automatically activated in order to continue recording the increasing or decreasing current.

Fig. 9 Experimentally obtained anodic polarization curve for Alloy F (6811-7). The break marks in the curve indicate where the resistance selector switch was automatically activated in order to continue recording the increasing or decreasing current.

Fig. 10 Experimentally obtained anodic polarization curve for Alloy G (6811-8). The break marks in the curve indicate where the resistance selector switch was automatically activated in order to continue recording the increasing or decreasing current.

Fig. 11 Experimentally obtained anodic polarization curve for Alloy H (6811-9). The break marks in the curve indicate where the resistance selector switch was automatically activated in order to continue recording the increasing or decreasing current.

Fig. 12 Experimentally obtained anodic polarization curve for Alloy I (6811-10). The break marks in the curve indicate where the resistance selector switch was automatically activated in order to continue recording the increasing or decreasing current.

Fig. 13 Experimentally determined anodic polarization curve for type 304 stainless steel in the as-received (annealed) condition.

Fig. 14 Experimentally determined anodic polarization curve for type 316 stainless steel in the as-received (annealed) condition.

Fig. 15 Photomicrograph of Alloy A (685-19) taken immediately after the polarization curve was obtained. Note the heavy intergranular attack. (160x).

Fig. 16 Photomicrograph of Alloy B (6811-3) taken immediately after the polarization curve was obtained. Note the relief effect caused by the highly distorted austenite. Compare the amount of intergranular attack with Fig. 15. (160x).

Fig. 17 Photomicrograph of Alloy C (6811-4) taken immediately after the polarization curve was obtained. Compare with Fig. 16. (160x).

Fig. 18 Photomicrograph of Alloy D (6811-6) taken immediately after the polarization curve was obtained. Compare with Fig. 17. (160x).

Fig. 19 Photomicrograph of Alloy F (6811-7) taken immediately after the polarization curve was obtained. Compare the amount of intergranular attack with Figs. 15 through 18. Some grains do not show the relief markings because of their different crystallographic orientations. (160x).

Fig. 20 Photomicrograph of Alloy G (6811-8) taken immediately after the polarization curve was obtained. Compare the amount of intergranular attack with Figs. 15 through 19. (160x).

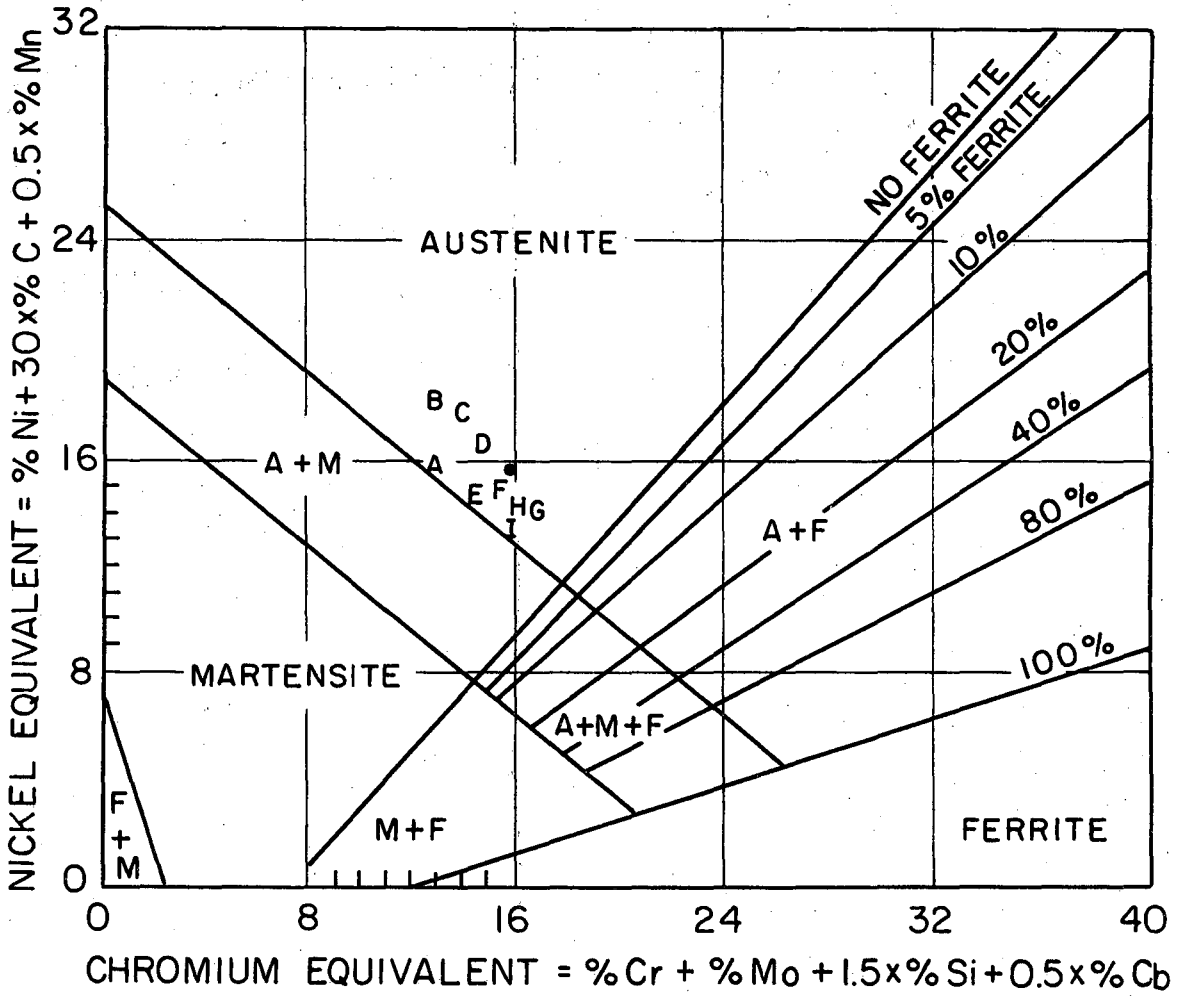
NICKEL EQUIVALENT = % Ni + 30 x % C + 0.5 x % Mn
CHROMIUM EQUIVALENT = % Cr + % Mo + 1.5 x % Si + 0.5 x % Cb
32
24
16
8
0
0
8
16
24
32
40
AUSTENITE
A + M
MARTENSITE
F + M
M + F
A + F
A + M + F
FERRITE
NO FERRITE
5% FERRITE
10%
20%
40%
80%
100%
A
B
C
D
E
F
G
H
I

FIG. 1

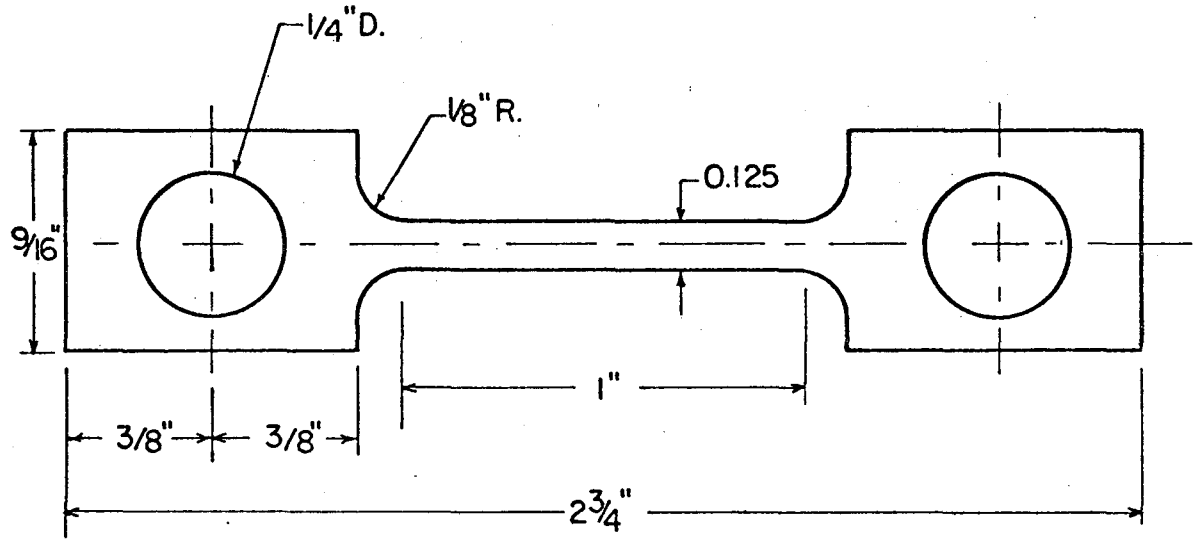

GAGE LENGTH = 1"

THICKNESS = 0.08"

SCALE: 2" - 1"

FIG. 2

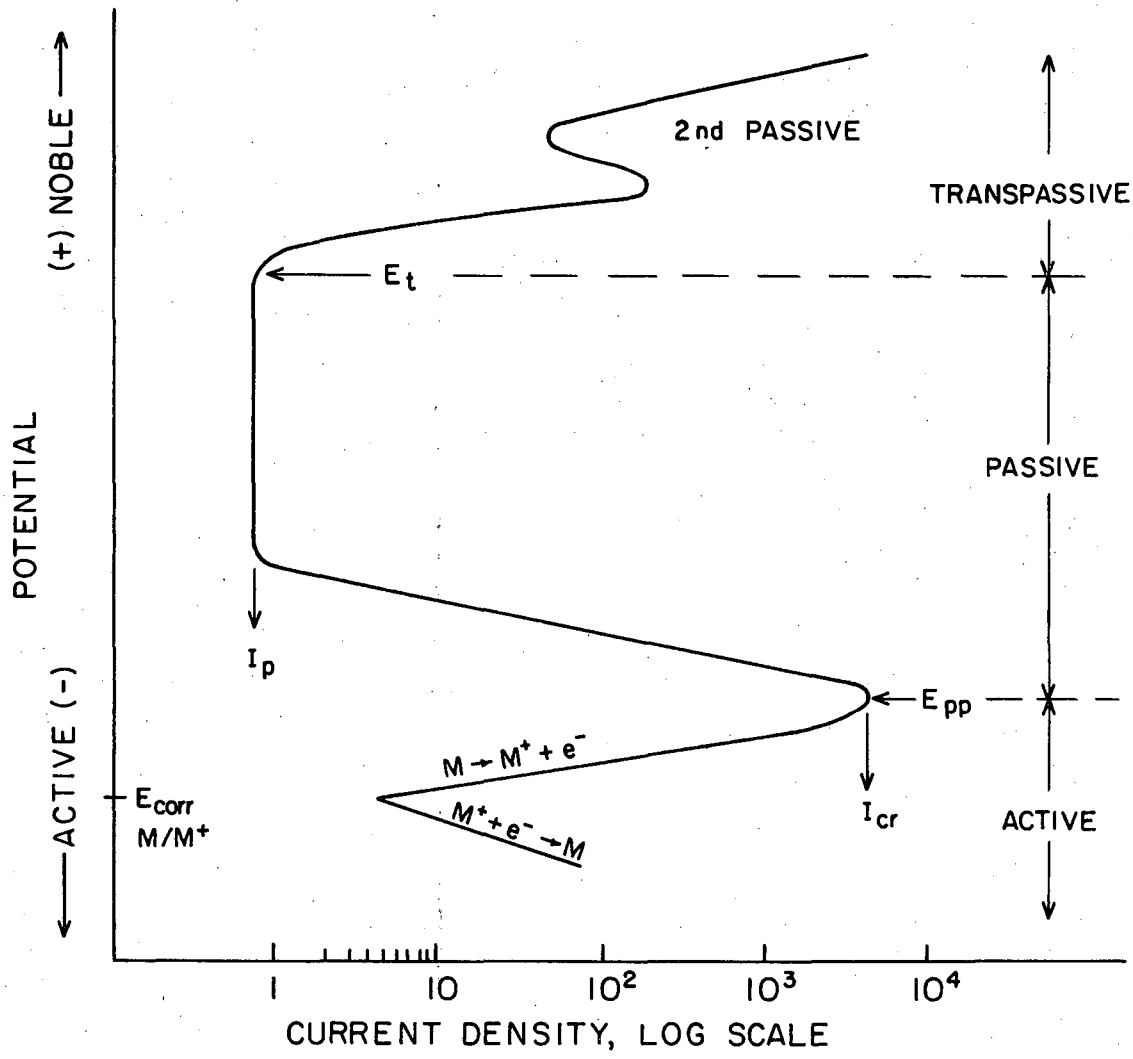

FIG. 3

XBL 698-1179

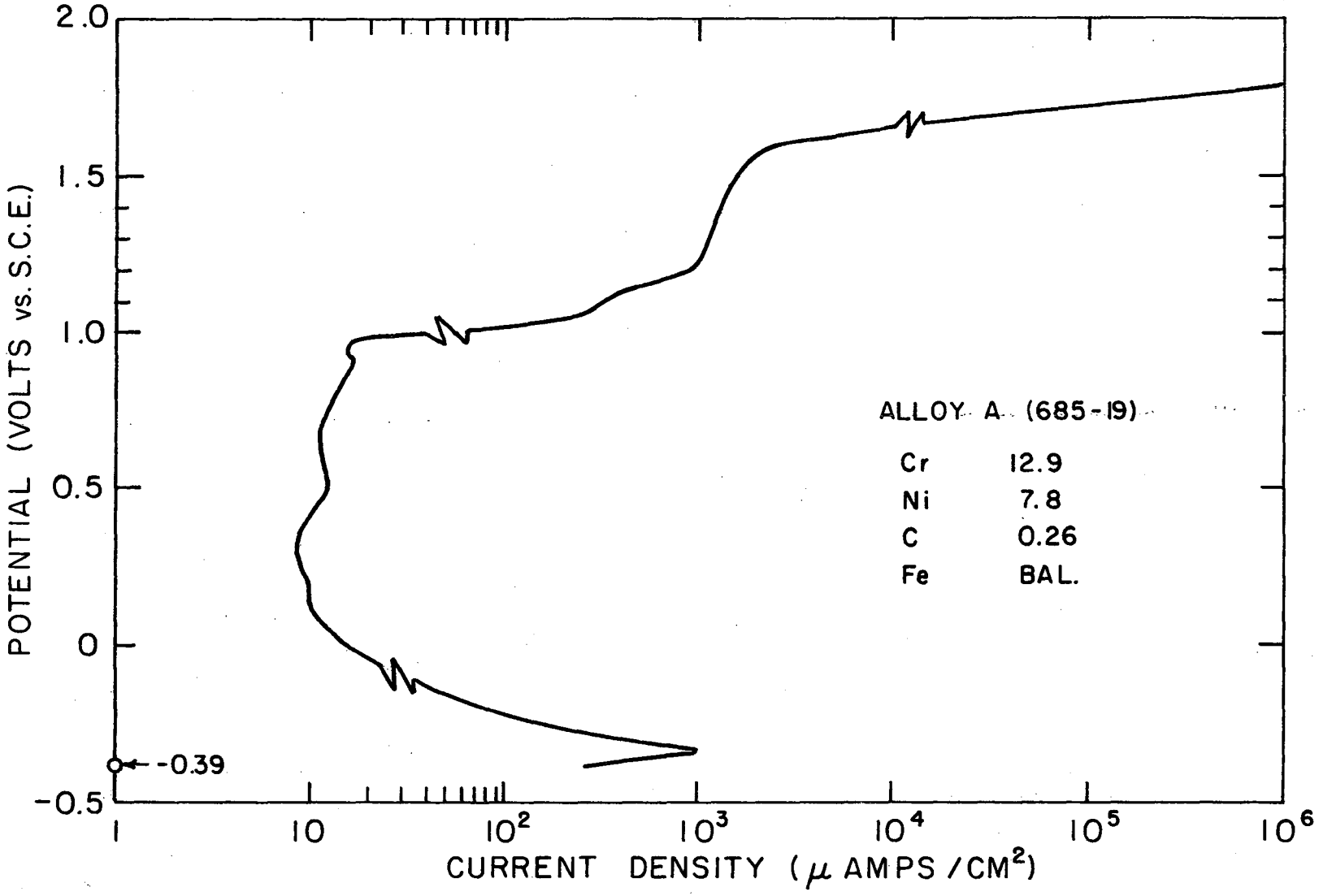
2.0
1.5
1.0
0.5
0
-0.5
POTENTIAL (VOLTS vs. S.C.E.)
-0.39
1
10
10^2
10^3
10^4
10^5
10^6
CURRENT DENSITY (μ AMPS / CM^2)
ALLOY A (685-19)
Cr 12.9
Ni 7.8
C 0.26
Fe BAL.

FIG. 4

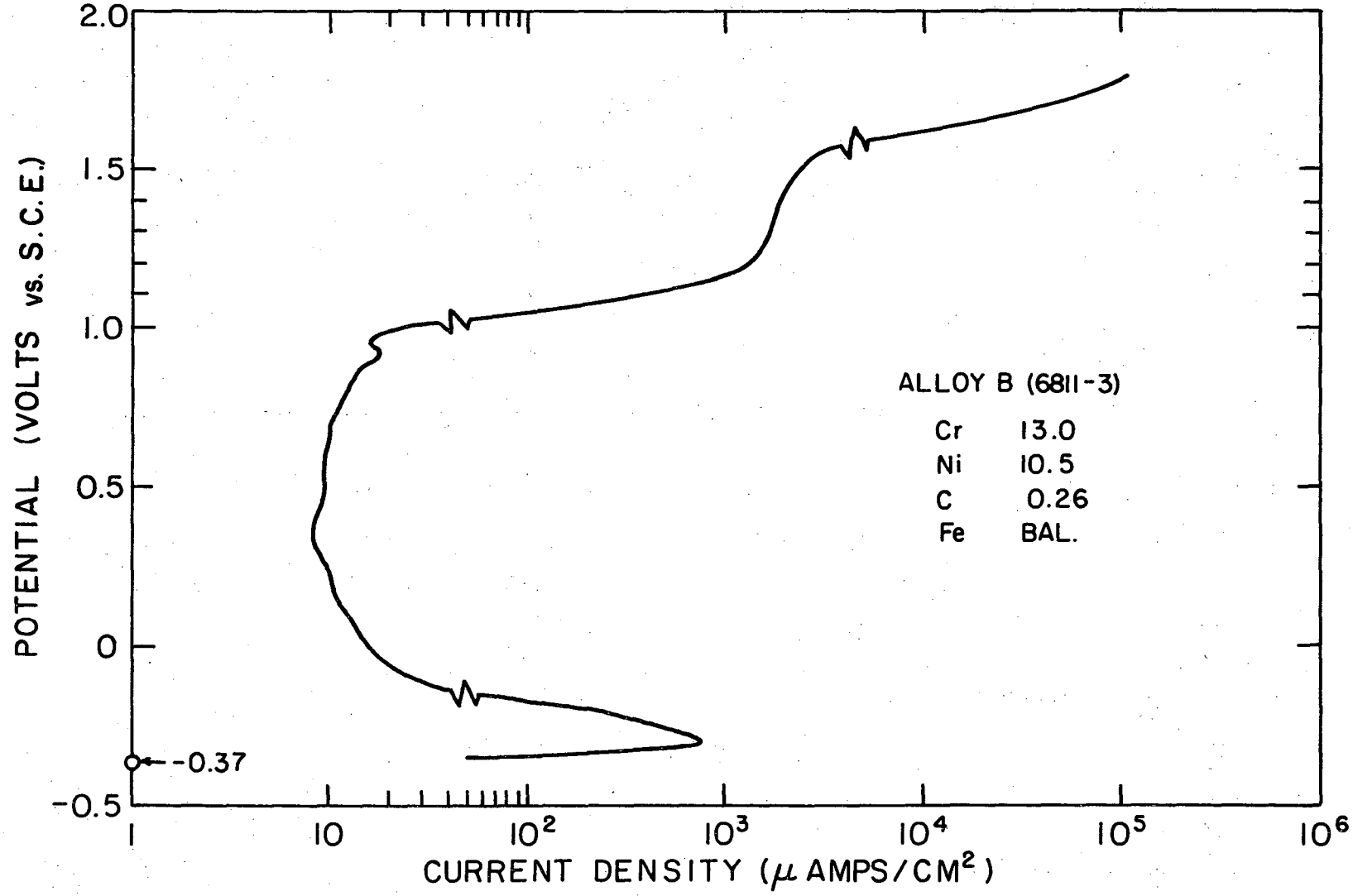
2.0
1.5
1.0
0.5
0
-0.5
POTENTIAL (VOLTS vs. S.C.E.)
-0.37
1
10
10^2
10^3
10^4
10^5
10^6
CURRENT DENSITY (μ AMPS/CM^2)
ALLOY B (6811-3)
Cr 13.0
Ni 10.5
C 0.26
Fe BAL.

FIG. 5

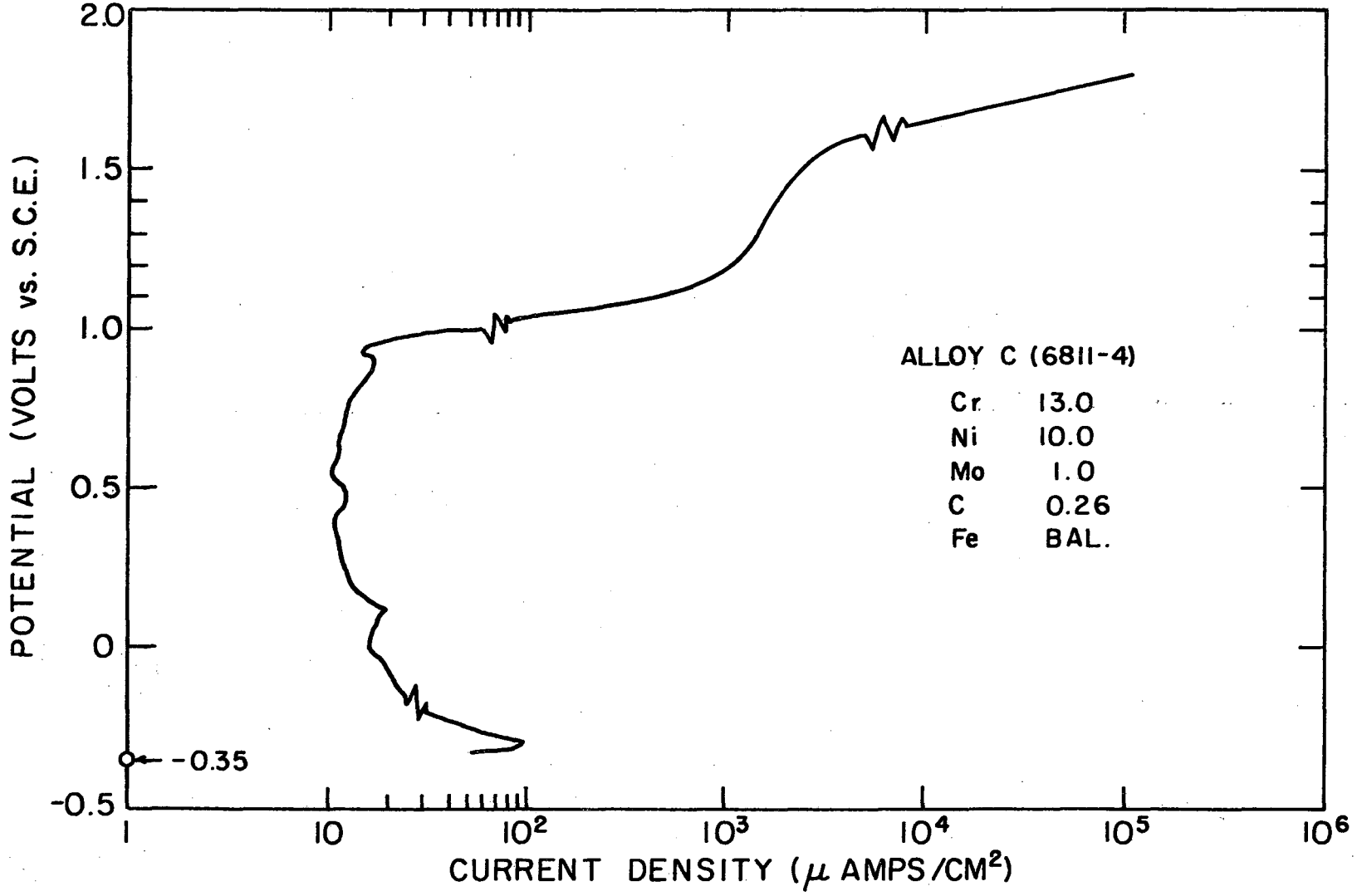
2.0
1.5
1.0
0.5
0
-0.5
POTENTIAL (VOLTS vs. S.C.E.)
-0.35
1
10
10²
10³
10⁴
10⁵
10⁶
CURRENT DENSITY (μ AMPS/CM²)
ALLOY C (6811-4)
Cr 13.0
Ni 10.0
Mo 1.0
C 0.26
Fe BAL.

FIG. 6

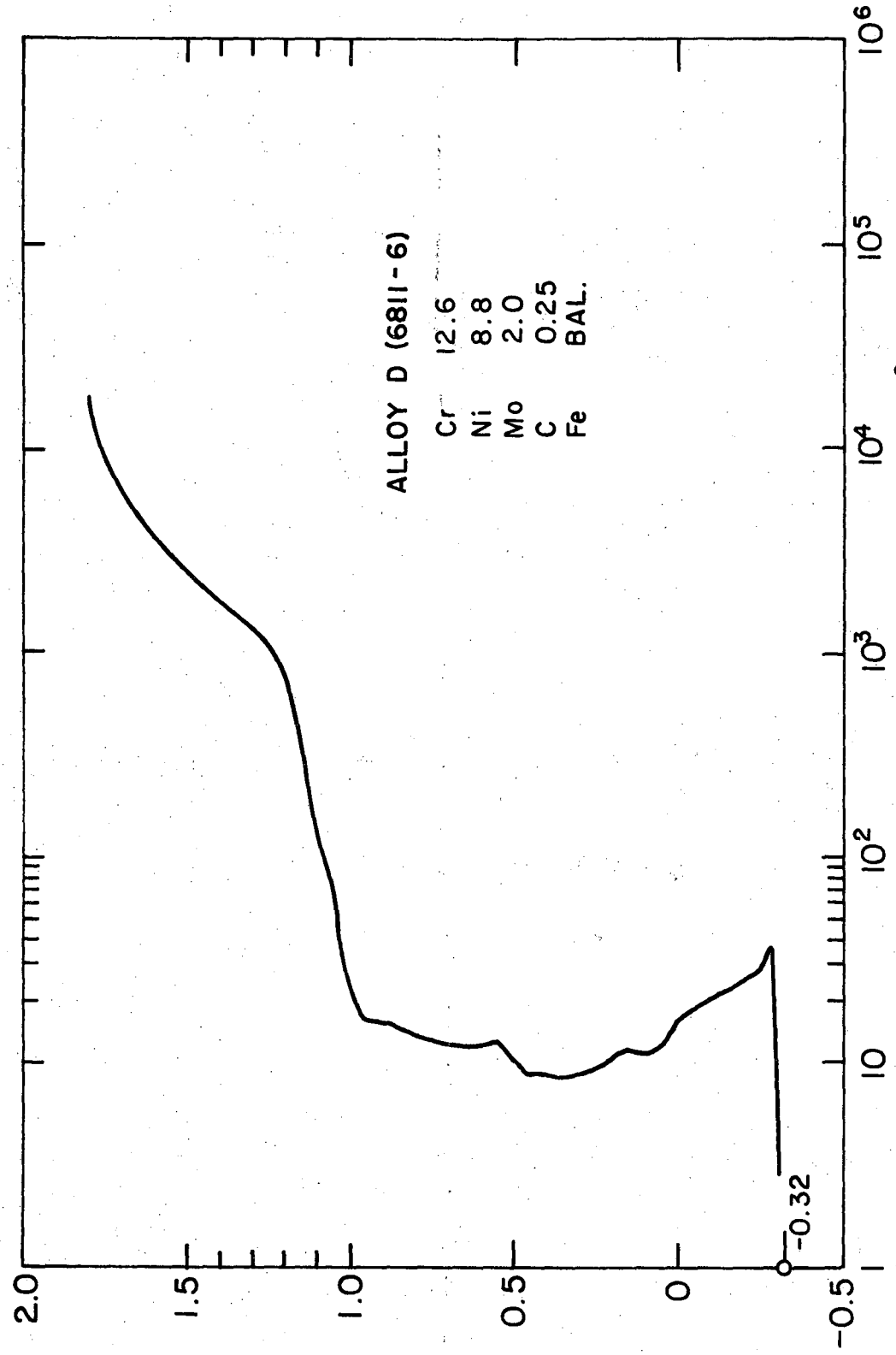
ALLOY D (6811-6)
Cr 12.6
Ni 8.8
Mo 2.0
C 0.25
Fe BAL.
-0.32
2.0
1.5
1.0
0.5
0
-0.5
1
10
10²
10³
10⁴
10⁵
10⁶
POTENTIAL (VOLTS vs. S.C.E.)
CURRENT DENSITY (μAMPS/CM²)

FIG. 7

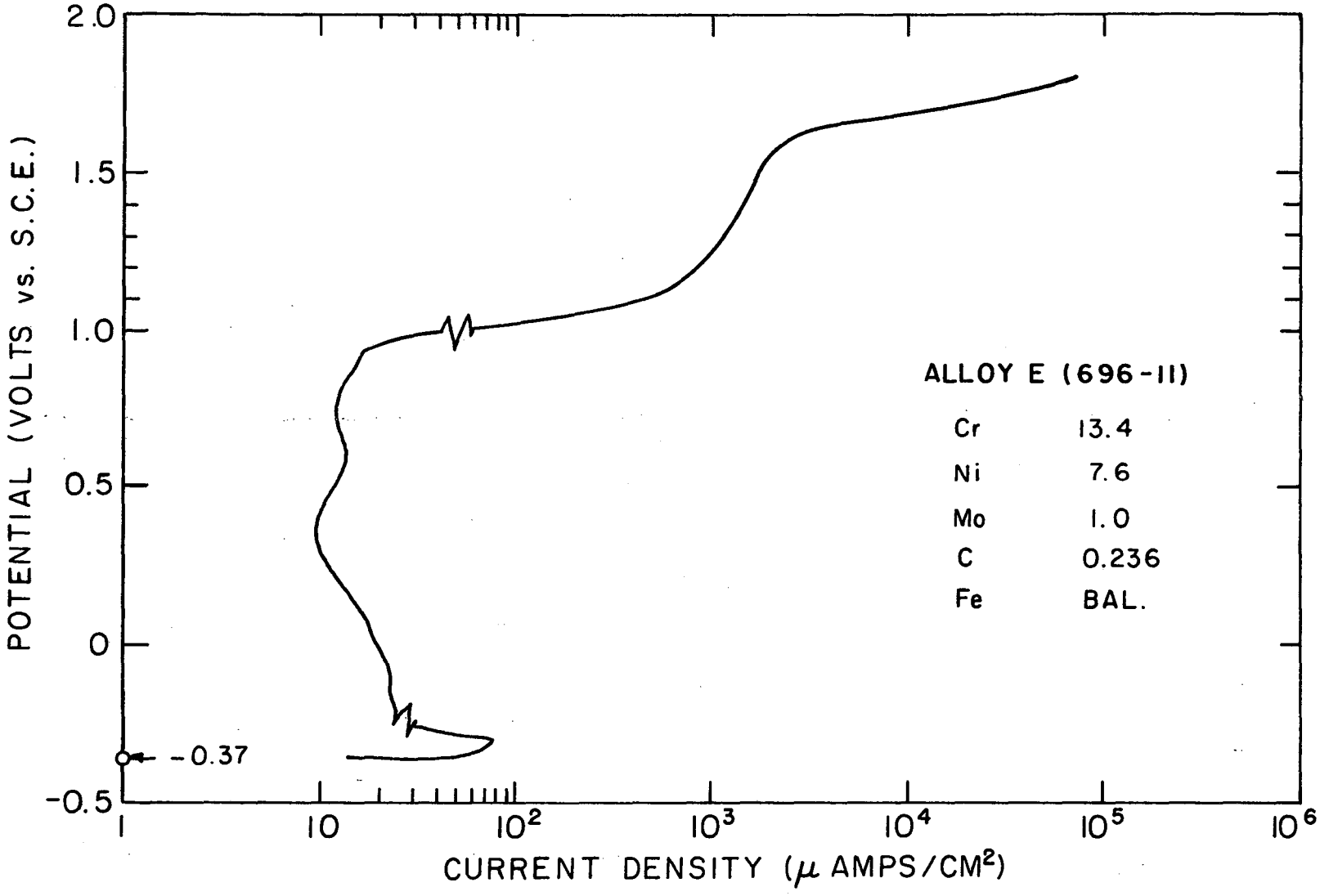
2.0
1.5
1.0
0.5
0
-0.5
POTENTIAL (VOLTS vs. S.C.E.)
-0.37
1
10
10^2
10^3
10^4
10^5
10^6
CURRENT DENSITY (μ AMPS/CM^2)
ALLOY E (696-11)
Cr 13.4
Ni 7.6
Mo 1.0
C 0.236
Fe BAL.

FIG. 8

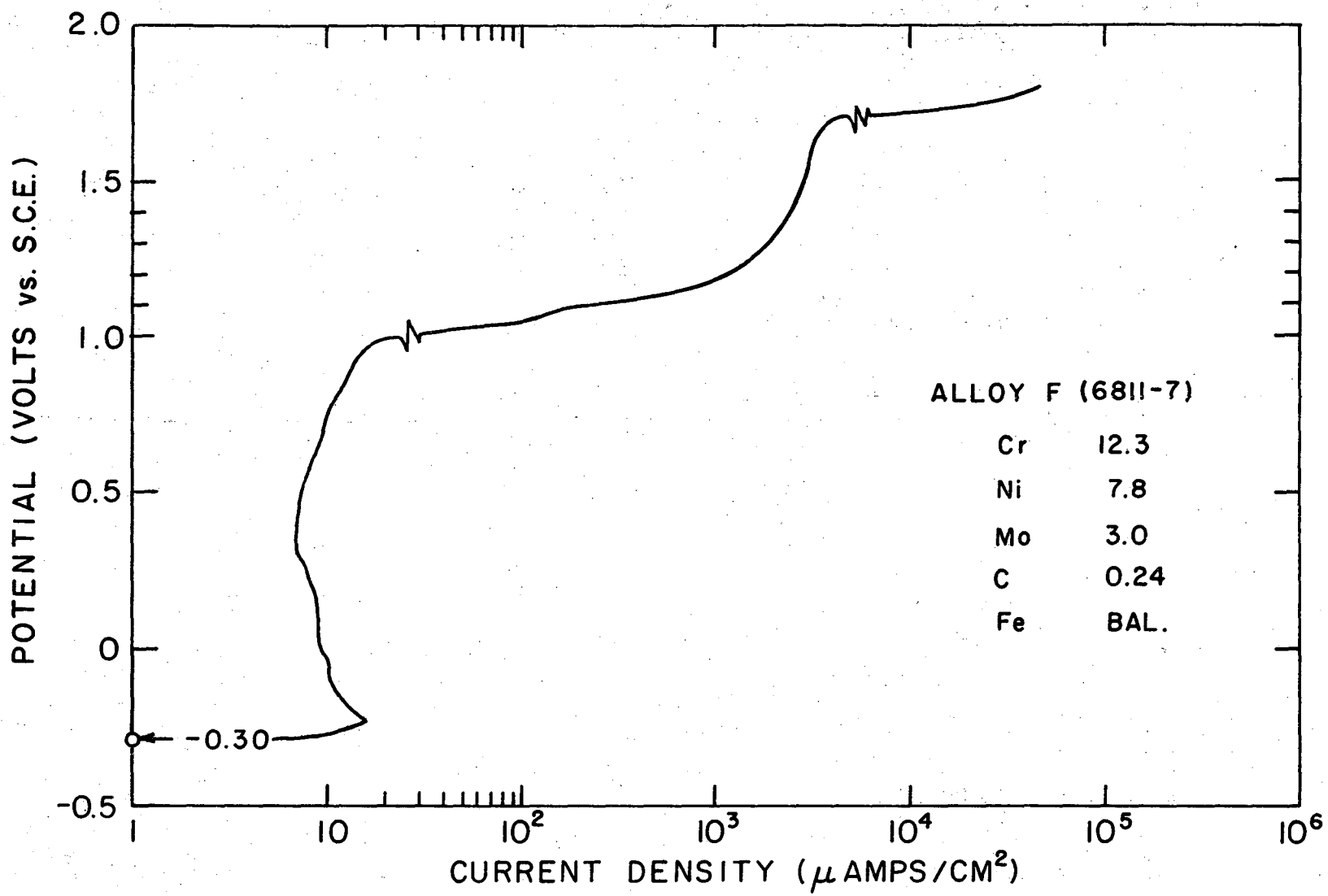
2.0
1.5
1.0
0.5
0
-0.5
POTENTIAL (VOLTS vs. S.C.E.)
-0.30
ALLOY F (6811-7)
Cr 12.3
Ni 7.8
Mo 3.0
C 0.24
Fe BAL.
1
10
10^2
10^3
10^4
10^5
10^6
CURRENT DENSITY (μAMPS/CM^2)

FIG. 9

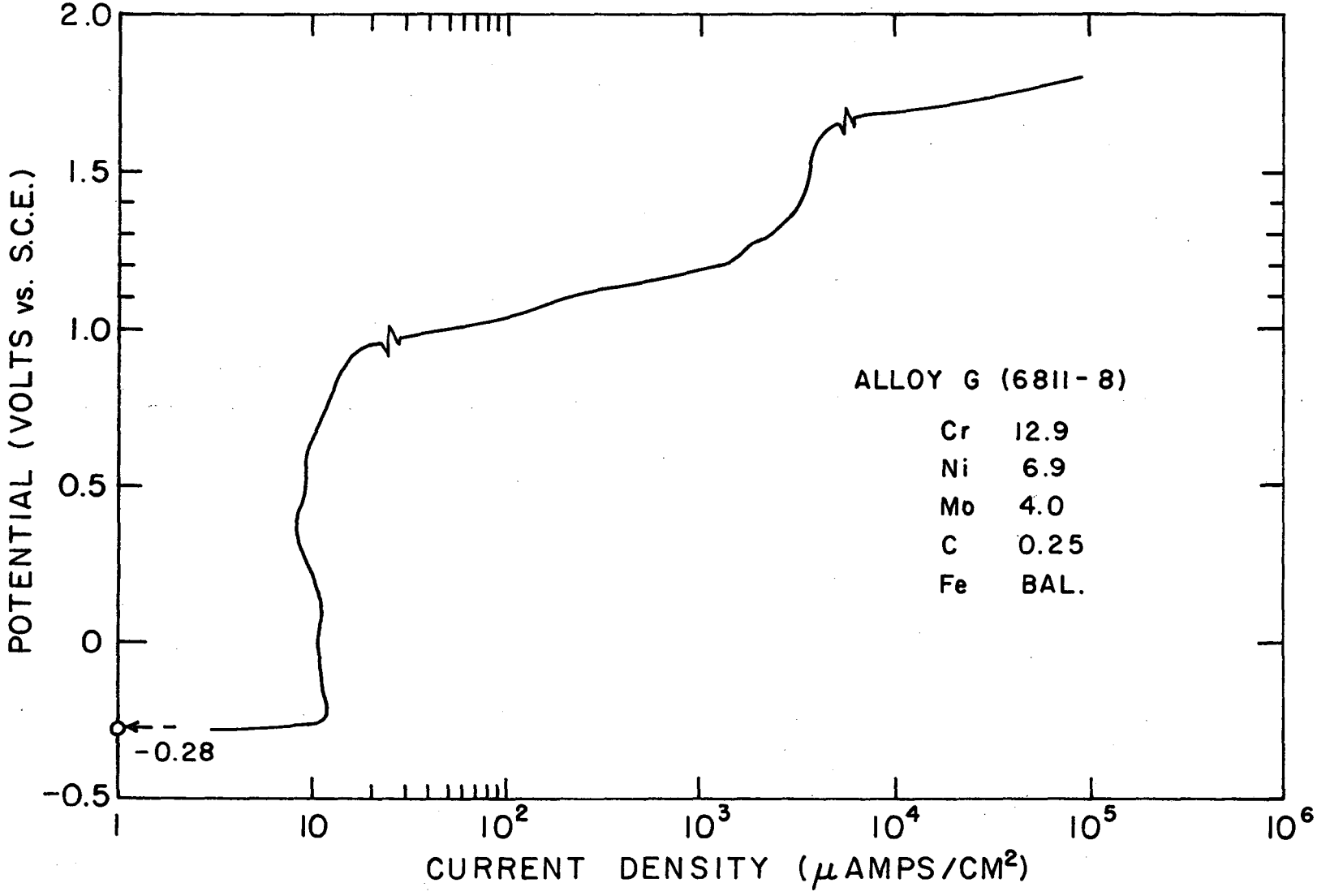
2.0
1.5
1.0
0.5
0
-0.5
POTENTIAL (VOLTS vs. S.C.E.)
-0.28
ALLOY G (6811-8)
Cr 12.9
Ni 6.9
Mo 4.0
C 0.25
Fe BAL.
1
10
10^2
10^3
10^4
10^5
10^6
CURRENT DENSITY (μAMPS/CM^2)

FIG. 10

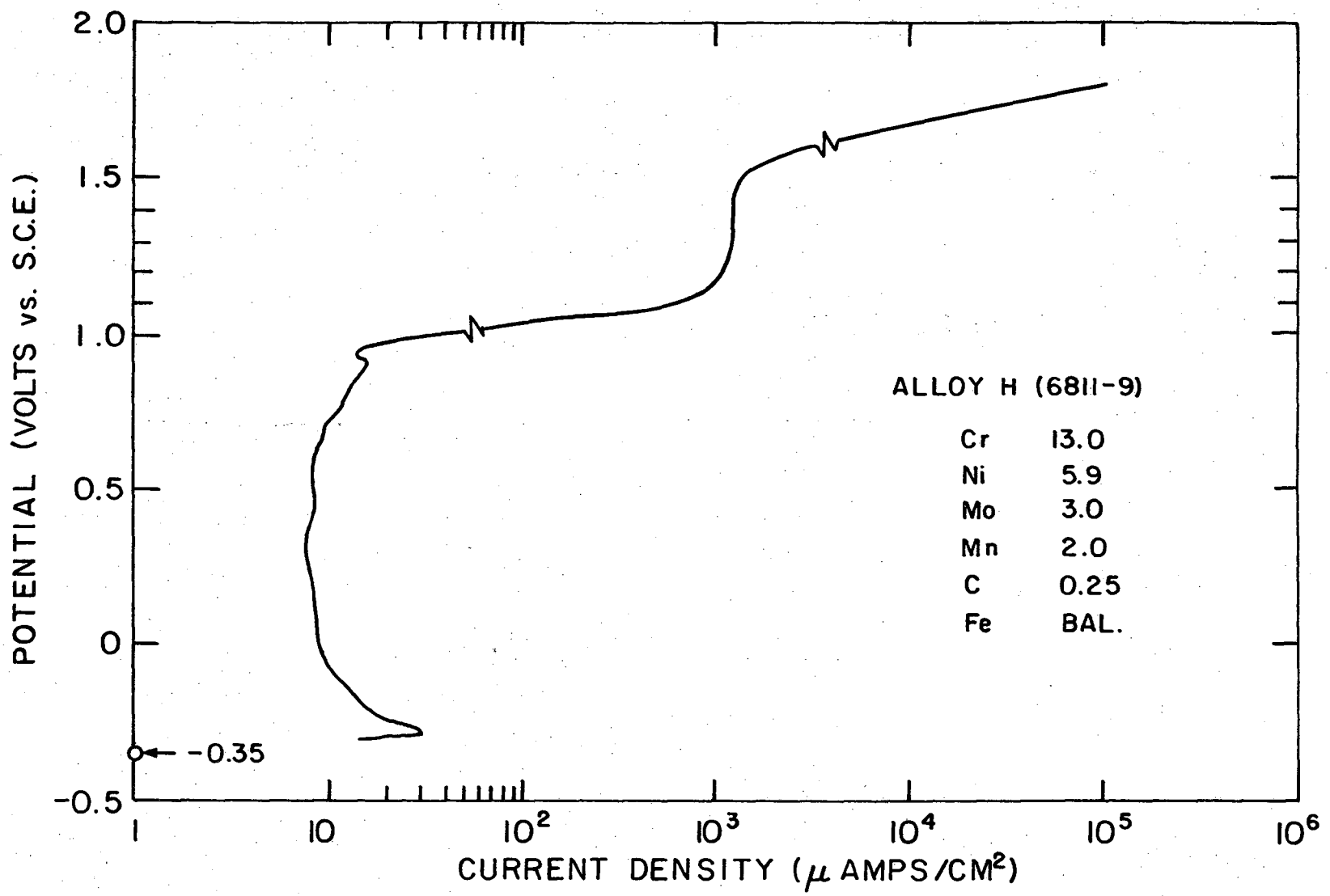
2.0
1.5
1.0
0.5
0
-0.5
POTENTIAL (VOLTS vs. S.C.E.)
-0.35
ALLOY H (6811-9)
Cr 13.0
Ni 5.9
Mo 3.0
Mn 2.0
C 0.25
Fe BAL.
1
10
10^2
10^3
10^4
10^5
10^6
CURRENT DENSITY (μ AMPS/CM^2)

FIG. 11

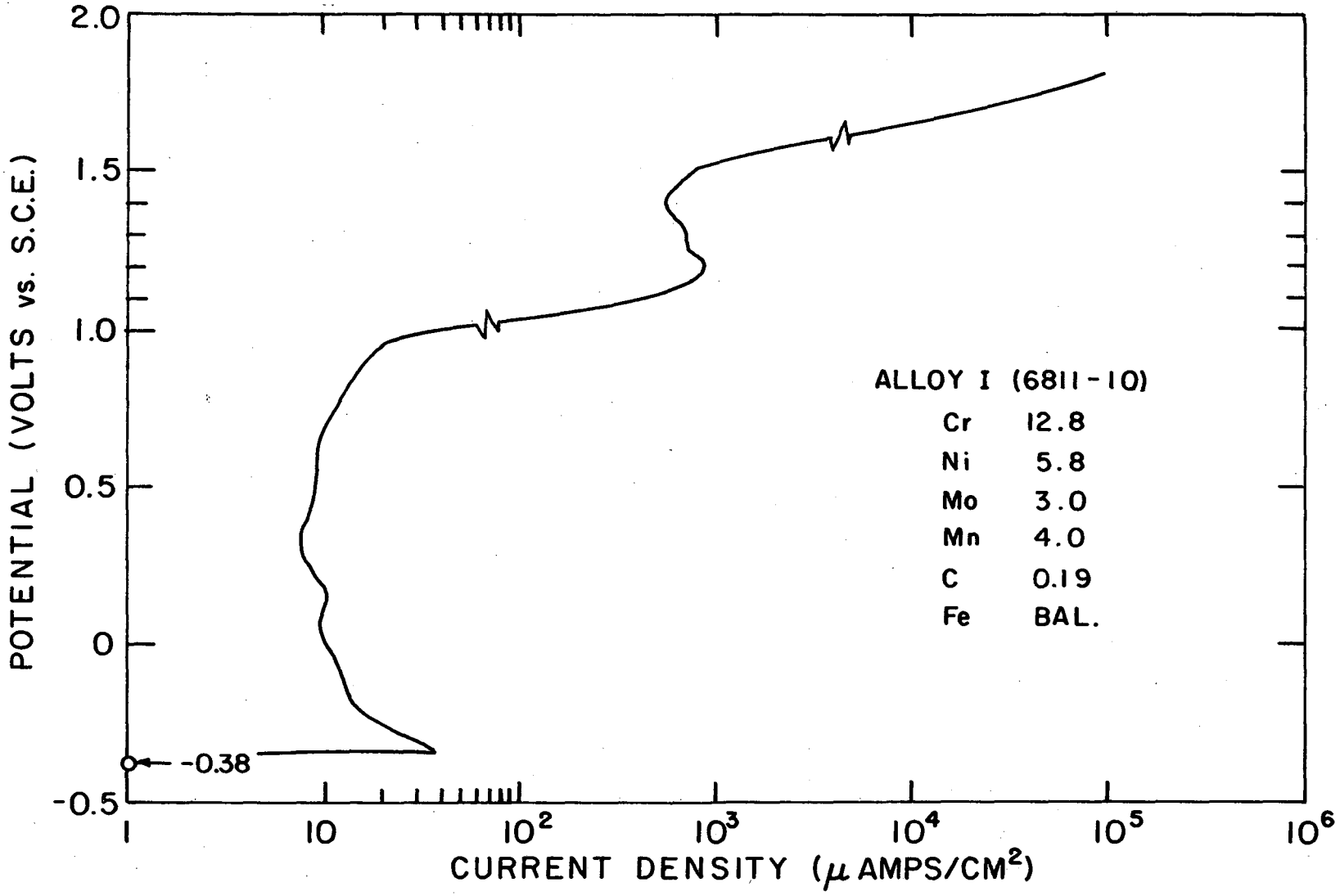
2.0
1.5
1.0
0.5
0
-0.5
POTENTIAL (VOLTS vs. S.C.E.)
-0.38
ALLOY I (6811-10)
Cr 12.8
Ni 5.8
Mo 3.0
Mn 4.0
C 0.19
Fe BAL.
1
10
10^2
10^3
10^4
10^5
10^6
CURRENT DENSITY (μ AMPS/CM^2)

FIG. 12

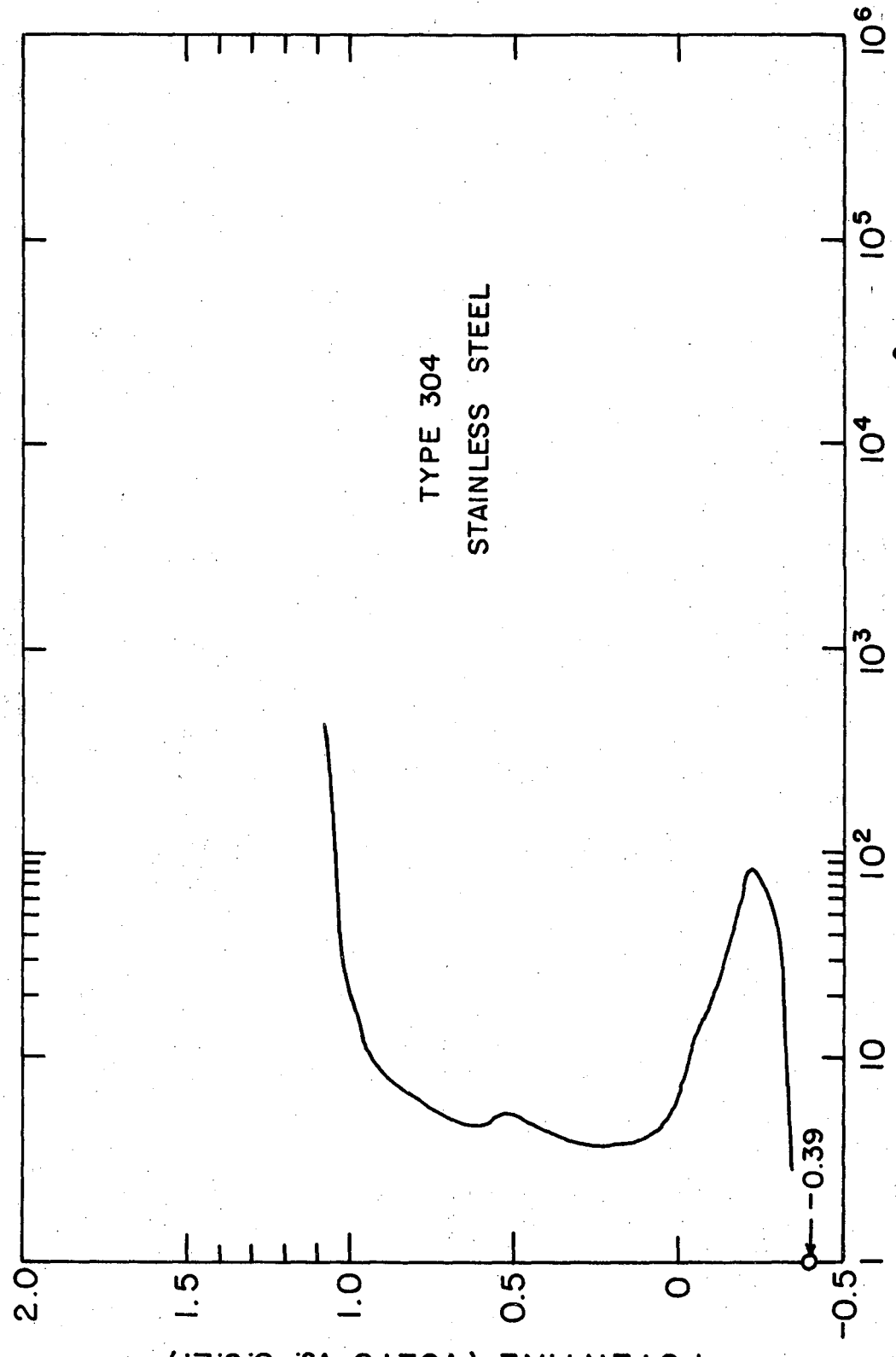
TYPE 304
STAINLESS STEEL
-0.39
2.0
1.5
1.0
0.5
0
-0.5
1
10
10²
10³
10⁴
10⁵
10⁶
POTENTIAL (VOLTS vs. S.C.E.)
CURRENT DENSITY (μ AMPS/CM²)

FIG. 13

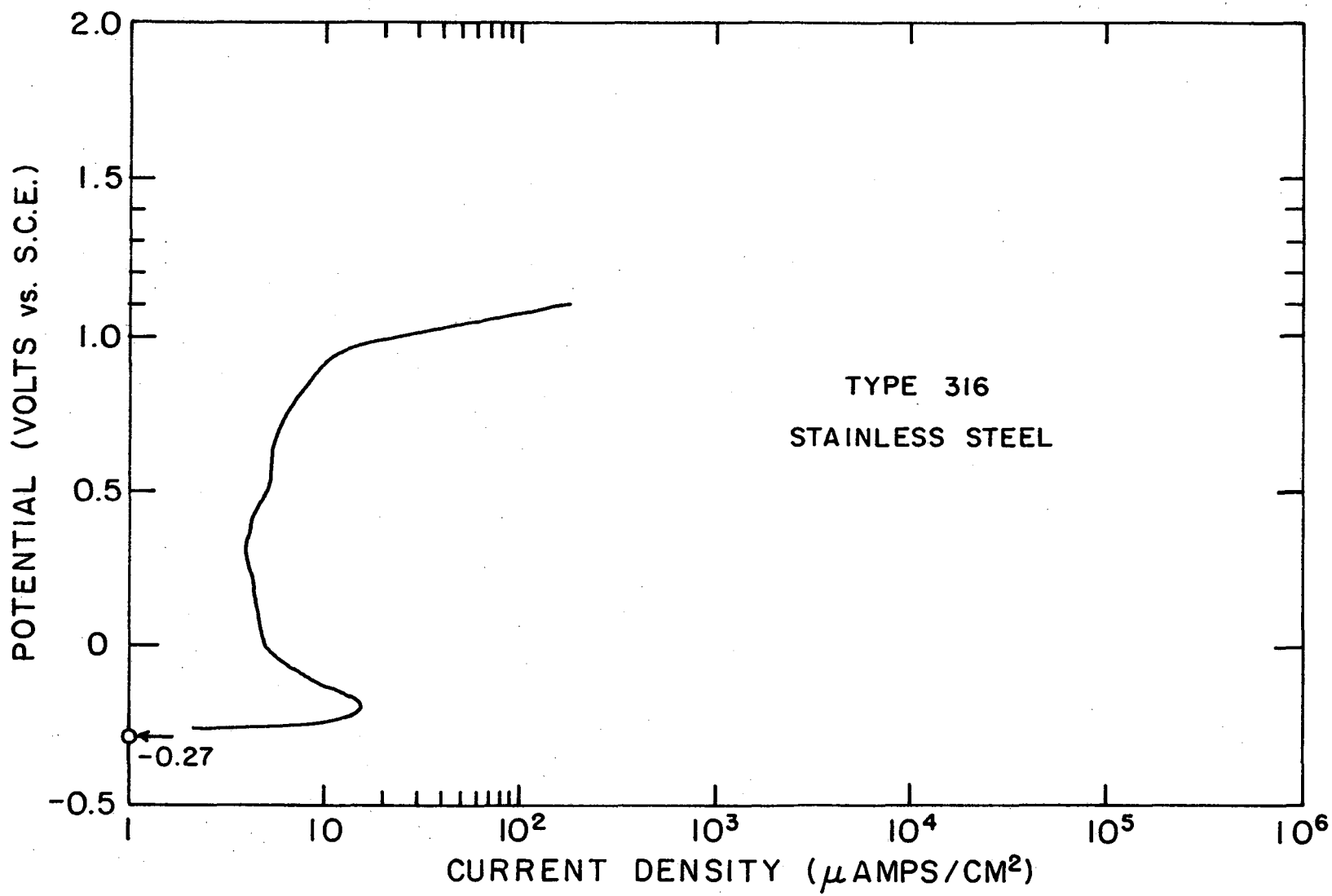
2.0
1.5
1.0
0.5
0
-0.5
POTENTIAL (VOLTS vs. S.C.E.)
-0.27
TYPE 316
STAINLESS STEEL
1
10
10^2
10^3
10^4
10^5
10^6
CURRENT DENSITY (μAMPS/CM^2)

FIG. 14

XBB 698-4961

Fig. 15

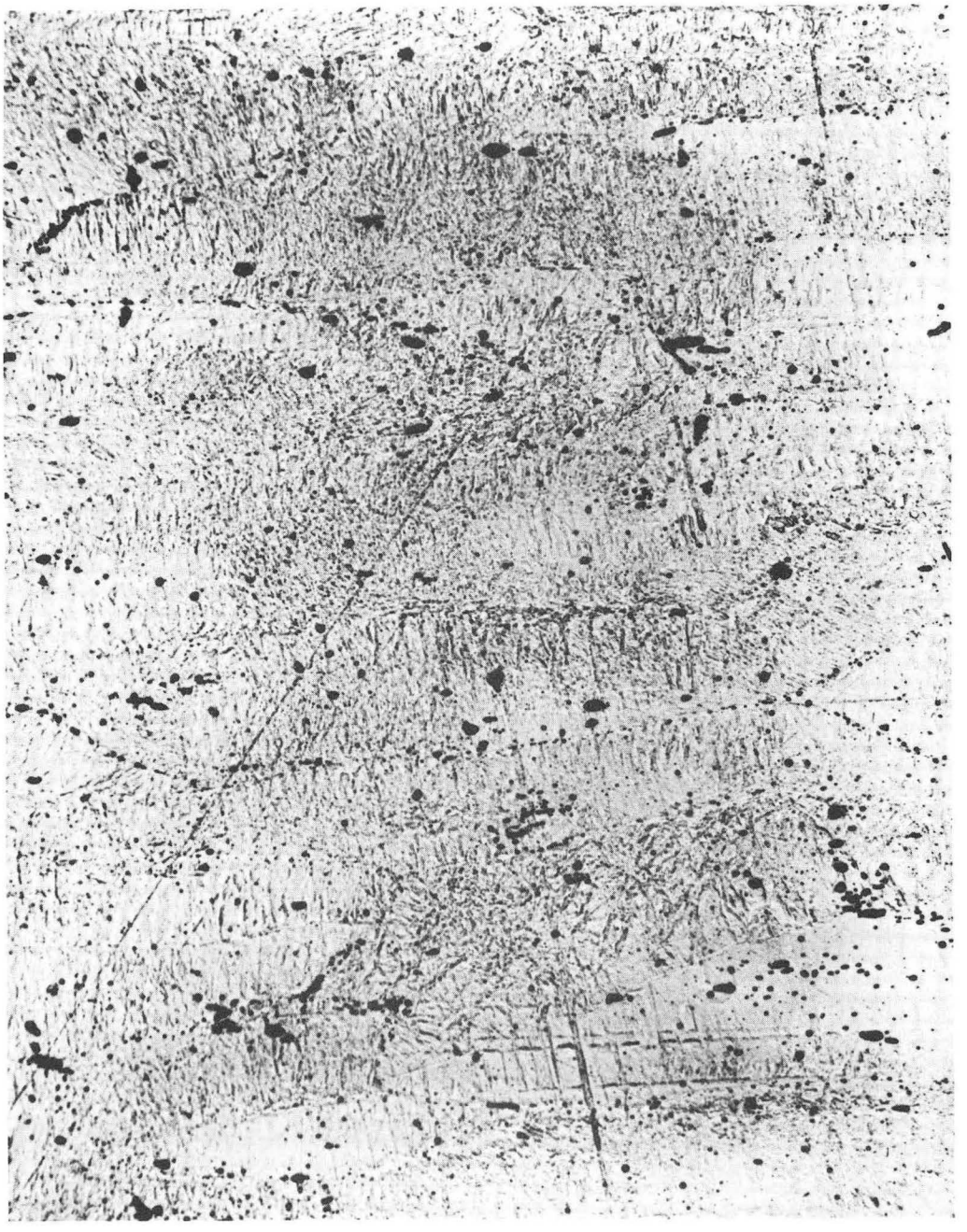

XBB 698-4962

Fig. 16

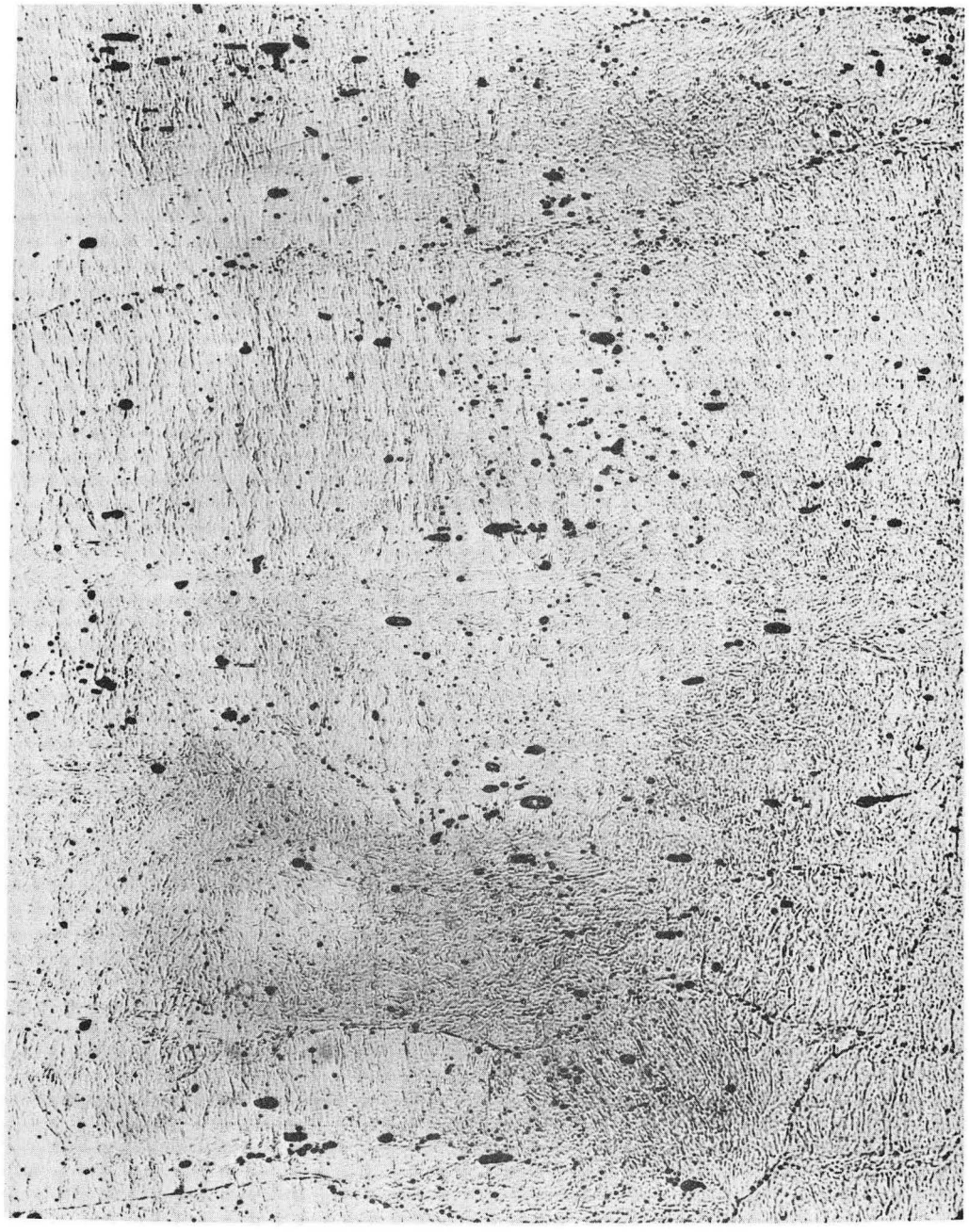

XBB 698-4963

Fig. 17

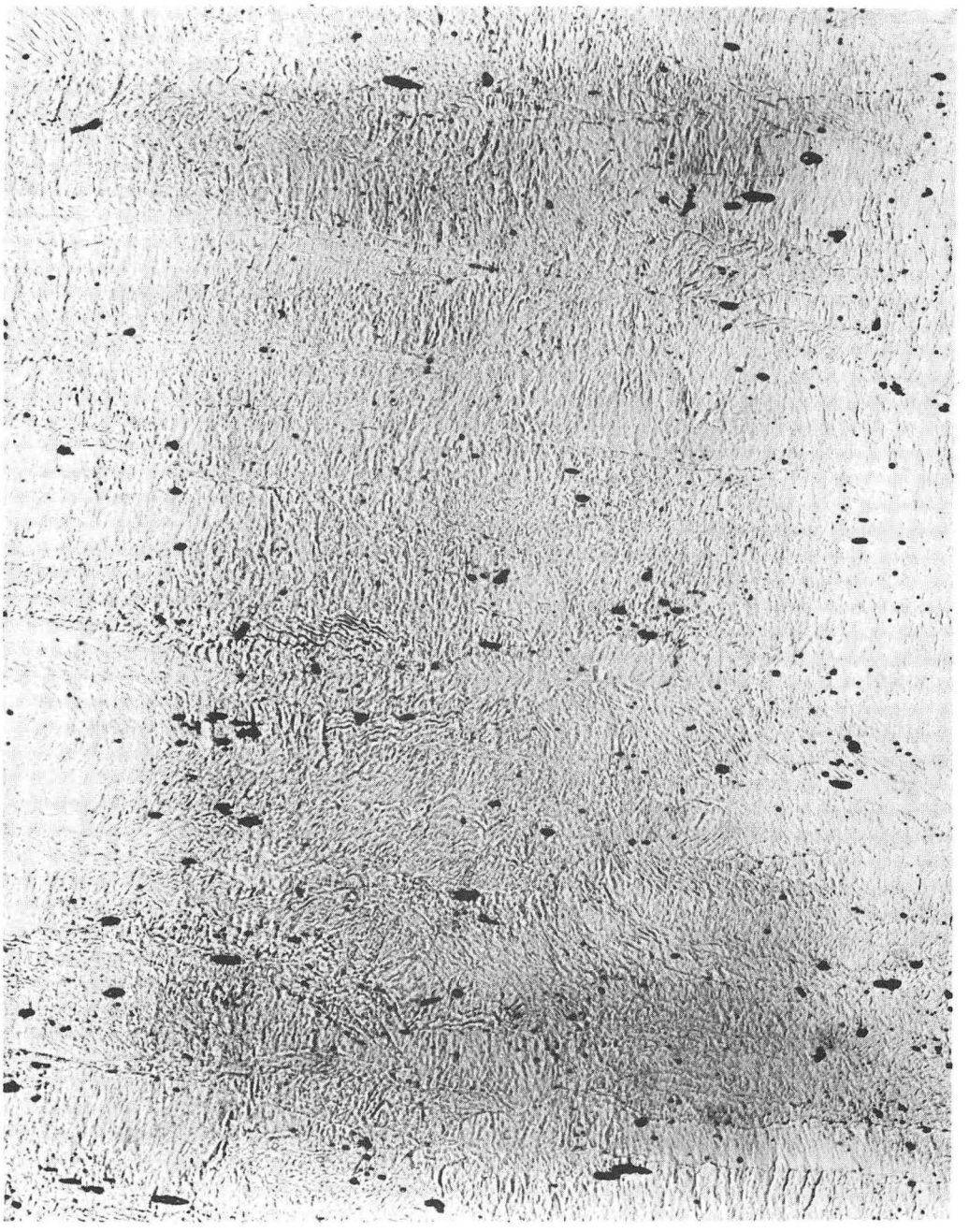

XBB 698-4964

Fig. 18

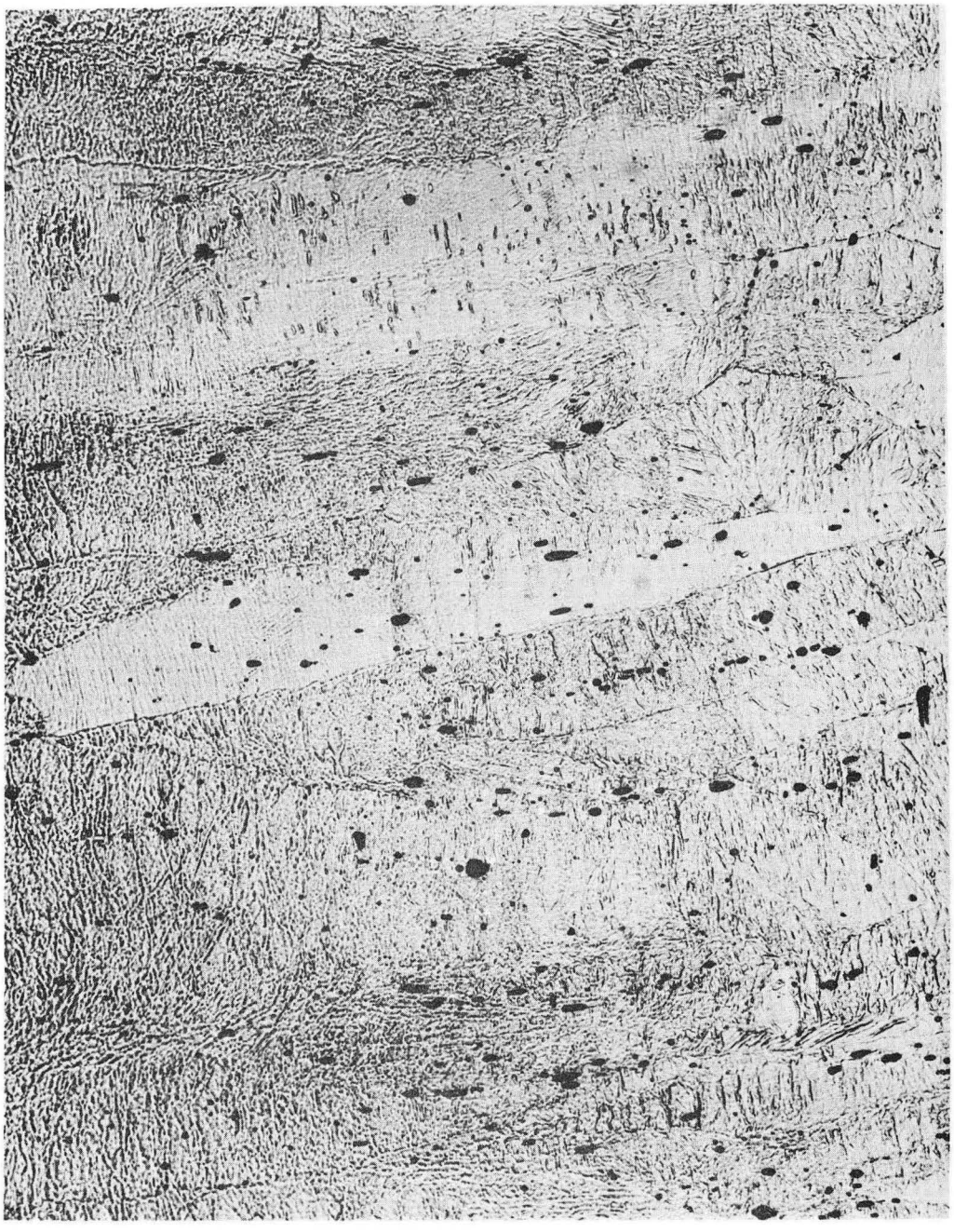

XBB 698-4965

Fig. 19

XBB 698-4966

Fig. 20

LEGAL NOTICE

This report was prepared as an account of Government sponsored work. Neither the United States, nor the Commission, nor any person acting on behalf of the Commission:

A. Makes any warranty or representation, expressed or implied, with respect to the accuracy, completeness, or usefulness of the information contained in this report, or that the use of any information, apparatus, method, or process disclosed in this report may not infringe privately owned rights; or

B. Assumes any liabilities with respect to the use of, or for damages resulting from the use of any information, apparatus, method, or process disclosed in this report.

As used in the above, "person acting on behalf of the Commission" includes any employee or contractor of the Commission, or employee of such contractor, to the extent that such employee or contractor of the Commission, or employee of such contractor prepares, disseminates, or provides access to, any information pursuant to his employment or contract with the Commission, or his employment with such contractor.

TECHNICAL INFORMATION DIVISION
LAWRENCE RADIATION LABORATORY
UNIVERSITY OF CALIFORNIA
BERKELEY, CALIFORNIA 94720